Synthesis, Vibrational Spectra, and Normal Mode Analysis of Nickel(II) 1,5-Dihydroxy-1,5-dimethyloctaethylbacteriochlorin: A Model for Bacteriochlorophylls

Songzhou Hu, Arka Mukherjee, and Thomas G. Spiro*

Contribution from the Department of Chemistry, Princeton University, Princeton, New Jersey 08544

Received June 18, 1993®

Abstract: Resonance Raman (RR) and FT-IR spectra are reported for nickel(II) 1,5-dihydroxy-1,5-dimethyloctaethylbacteriochlorin [Ni(HOEBC)] and its *meso*-d_4 isotopomer. All the in-plane skeletal RR-active modes and most IR-active modes are assigned with the aid of a normal mode analysis by using a force field developed for nickel(II) octaethylporphyrin and by scaling the bond stretch force constants to bond lengths revealed in the crystal structure of nickel(II) octaethylbacteriochlorin. The calculated eigenvectors provide insight into the essential vibrational characteristics of metallobacteriochlorins. The RR spectra of Ni(HOEBC) were acquired with a variety of excitation wavelengths, near resonance with the B_x, Q_x, and Q_y transitions. The enhancement pattern of the observed RR intensities reveals that the B_x- and near-Q_y-resonant spectra are dominated by Franck-Condon-active modes while the Q_x-resonant spectrum is dominated by vibronically active modes. The B_x-resonant spectrum also shows significant vibronic scattering, via coupling between the B_x- and B_y-excited states. Frequencies correlate well among Ni(II) complexes of octaethylporphine (OEP) and hydroporphyrins for modes containing similar local mode contributions, when allowance is made for C_β–C_β bond order reduction and the effects of symmetry lowering. Assignments are proposed for the existing RR data on bacteriochlorophyll a.

Introduction

There is increasing interest in understanding the structural and dynamic properties of bacteriochlorophylls, a class of tetrahydroporphyrin derivatives that play a vital role in light harvesting, energy transduction, and charge separation in the purple photosynthetic bacteria.[1] While the determination of the three-dimensional crystal structure of the reaction center complexes from *Rhodopseudomonas viridis*[2] and *Rhodobacter sphaeroides*[3] has provided a unique opportunity to visualize the spatial arrangements of chromophores along the light-induced electron-transfer path, a better understanding of this process will require detailed elucidation of the electronic and molecular structures of these pigments and their interactions with the proteins. Because of its high sensitivity and selective enhancement for the vibrational modes of chromophores, resonance Raman (RR) spectroscopy[4,5] is a particularly powerful probe of chromophore structure and has been increasingly applied to investigate the ground-state, excited-state, and π cation radical species of chlorophylls[6] and bacteriochlorophylls.[7] When excited in resonance with the π–π^* transitions, these photosynthetic pigments give rise to very rich RR spectra. However, previous studies on photosynthetic reaction centers have been generally limited to the analysis of the carbonyl ν(C=O) stretching and a few high-frequency modes.[8] To fully exploit the structural information contained in the RR spectra, it is essential to understand the normal mode characteristics of the core metallobacteriochlorin and bacteriochlorophyll structures, in order to properly assign the observed spectral features.

Normal modes have been extensively characterized for metallochlorins[9-14] and metalloisobacteriochlorins,[15-17] but there

* Abstract published in *Advance ACS Abstracts*, November 15, 1993.

(1) Scheer, H., Ed. *Chlorophylls*; CRC: Boca Raton, FL, 1991.

(2) (a) Deisenhofer, J.; Epp, O.; Miki, K.; Huber, R.; Michel, H. *J. Mol. Biol.* **1984**, *180*, 385–398. (b) Deisenhofer, J.; Epp, O.; Miki, K.; Huber, R.; Michel, H. *Nature* **1985**, *318*, 618–624.

(3) (a) Allen, J. P.; Feher, G.; Yeates, T. O.; Komiya, H.; Rees, D. C. *Proc. Natl. Acad. Sci. U.S.A.* **1987**, *84*, 5730–5734, (b) 6162–6166. (c) Yeates, T. O.; Komiya, H.; Rees, D. C.; Allen, J. P.; Feher, G. *Proc. Natl. Acad. Sci. U.S.A.* **1987**, *84*, 6438–6442. (d) Allen, J. P.; Feher, G.; Yeates, T. O.; Komiya, H.; Rees, D. C. *Proc. Natl. Acad. Sci. U.S.A.* **1988**, *85*, 8587–8491.

(4) Spiro, T. G., Ed. *Biological Applications of Raman Spectroscopy*; Wiley: New York, 1988; Vol. III.

(5) For recent reviews on RR spectroscopy of tetrapyrrole-derived chromophores, see: (a) Lutz, M. In *Advanced Infrared Raman Spectroscopy* Clark, R. J. H., Hester, R. E., Eds.; Wiley: New York, 1984; Vol. 11, pp 211–300. (b) Abe, M. In *Advances in Spectroscopy*; Clark, R. J. H., Hester, R. E., Eds.; Wiley: New York, 1986; Vol. 12, pp 347–393. (c) Kitagawa, T.; Ozaki, Y. *Struct. Bonding (Berlin)* **1987**, *64*, 71–114. (d) Schick, G. A.; Bocian, D. F. *Biochim. Biophys. Acta* **1987**, *895*, 127–154. (e) Spiro, T. G.; Czernuszewicz, R. S.; Li, X.-Y. *Coord. Chem. Rev.* **1990**, *100*, 541–571. (f) Lutz, M.; Mantele, W. In *Chlorophylls*; Scheer, H., Ed.; 1991; pp 855–902. (g) Procyk, A. D.; Bocian, D. F. *Annu. Rev. Phys. Chem.* **1992**, *43*, 456–496.

(6) (a) Lutz, M.; Breton, J. *Biochem. Biophys. Res. Commun.* **1973**, *53*, 413–418. (b) Fujiwara, M.; Tasumi, M. *J. Phys. Chem.* **1986**, *90*, 250–255, 5646–5650. (c) Andersson, L. A.; Loehr, T. M.; Cotton, T. M.; Simpson, D. J.; Smith, K. M. *Biochim. Biophys. Acta* **1989**, *974*, 163. (d) Krawczyk, S. *Biochim. Biophys. Acta* **1989**, *976*, 140–149. (e) Koningstein, J. A.; Mattioli, T. A. *J. Phys. Chem.* **1989**, *93*, 5349–5351. (f) Thomas, L. L.; Kim, J.-H.; Cotton, T. M. *J. Am. Chem. Soc.* **1990**, *112*, 9378–9386. (g) Picorel, R.; Bakhtiari, M.; Lu, T.; Cotton, T. M.; Seibert, M. *Photochem. Photobiol.* **1992**, *56*, 263–270. (h) Hildebrandt, P.; Spiro, T. G. *J. Phys. Chem.* **1988**, *92*, 3355–3360.

(7) (a) Lutz, M.; Kleo, J. *Biochem. Biophys. Res. Commun.* **1976**, *69*, 711–717. (b) Lutz, M.; Kleo, J. *Biochim. Biophys. Acta* **1979**, *546*, 365–369. (c) Lutz, M; Hoff, A.; Brehamet, L. *Biochim. Biophys. Acta* **1982**, *679*, 331–341. (d) Cotton, T. M.; Van Duyne, R. P. *Biochem. Biophys. Res. Commun.* **1978**, *82*, 424–433. (e) Cotton, T. M.; Parks, K. D.; Van Duyne, R. P. *J. Am. Chem. Soc.* **1980**, *102*, 6399–6407. (f) Cotton, T. M.; Van Duyne, R. P. *J. Am. Chem. Soc.* **1981**, *103*, 6020–6026. (g) Callahan, P. M.; Cotton, T. M. *J. Am. Chem. Soc.* **1987**, *109*, 7001–7007. (h) Donohoe, R. J.; Frank, H. A.; Bocian, D. F. *Photochem. Photobiol.* **1988**, *48*, 531–537. (i) Nishizawa, E.; Koyama, Y. *Chem. Phys. Lett.* **1990**, *172*, 317–322. (j) Nishizawa, E.; Koyama, Y. *Chem. Phys. Lett.* **1991**, *176*, 390–394. (k) Donohoe, R. J.; Dyer, R. B.; Swanson, B. I.; Violette, C. A.; Frank, H. A.; Bocian, D. F. *J. Am. Chem. Soc.* **1990**, *112*, 6716–6718. (l) Shreve, A. P.; Cherepy, N. J.; Franzen, S.; Boxer, S. G.; Mathies, R. A. *Proc. Natl. Acad. Sci. U.S.A.* **1991**, *88*, 11207–11211. (m) Palaniappan, V.; Aldema, M. A.; Frank, H. A.; Bocian, D. F. *Biochemistry* **1992**, *31*, 11050–11058.

(8) (a) Robert, B.; Lutz, M. *Biochim. Biophys. Acta* **1985**, *807*, 10–23. (b) Zhou, Q.; Robert, B.; Lutz, M. *Biochim. Biophys. Acta* **1987**, *890*, 368–376. (c) Robert, B.; Frank, H. A. *Biochim. Biophys. Acta* **1988**, *934*, 401–405. (d) Robert, B.; Lutz, M. *Biochemistry* **1988**, *27*, 5108–5114. (e) Zhou, Q.; Robert, B.; Lutz, M. *Biochim. Biophys. Acta* **1989**, *977*, 10–18. (f) Peloquin, C. A.; Violette, C. A.; Frank, H. A.; Bocian, D. F. *Biochemistry* **1990**, *29*, 4892–4898. (g) Robert, R. *Biochim. Biophys. Acta* **1990**, *1017*, 99–111. (h) Picorel, R.; Holt, R. E.; Heald, R.; Cotton, T. M.; Seibert, M. *J. Am. Chem. Soc.* **1991**, *113*, 2839–2843. (i) Peloquin, J. M.; Bylina, E. J.; Youvan, D. C.; Bocian, D. F. *Biochim. Biophys. Acta* **1991**, *1056*, 85–88. (j) Mattioli, T. A.; Hoffmann, A.; Robert, B.; Schrader, B.; Lutz, M. *Biochemistry* **1991**, *30*, 4648–4654.

0002-7863/93/1515-12366$04.00/0

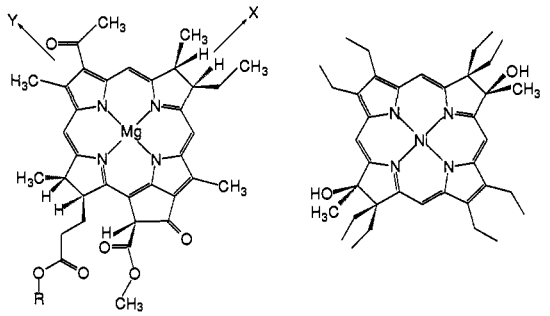

Figure 1. Molecular structures of bacteriochlorophyll a (left) and Ni-(HOEBC) (right).

has only been one study on a metallobacteriochlorin, namely copper *meso*-tetraphenylbacteriochlorin.[13b] Physiological bacteriochlorins, however, are substituted at the pyrrole β positions. β-substituted bacteriochlorins are difficult to prepare. The conventional synthetic method[18] of reducing octaethylporphine (OEP) with sodium in isoamyl alcohol produces octaethylchlorin (OEC) and octaethylisobacteriochlorin (OEiBC), but only trace amounts of extremely air- and light-sensitive octaethylbacteriochlorin (OEBC), which has been characterized only by its electronic absorption spectrum. It occurred to us that β-substituted bacteriochlorin can be obtained as a more stable alkylated octaethylbacteriochlorin by methylating 1,5-dioxooctaethylbacteriochlorin, which is conveniently synthesized from OEP via two different routes.[19] We have prepared the resulting 1,5-dihydroxy-1,5-dimethyloctaethylbacteriochlorin (HOEBC) and have obtained the RR and IR spectra of its nickel(II) complex and its *meso*-d_4 isotopomer. With the aid of a normal mode analysis and the selective RR enhancement pattern obtained with various excitation wavelengths, we have been able to assign most of the in-plane skeletal vibrations of Ni(HOEBC). This work is part of a systematic vibrational analysis of the nickel(II) complexes

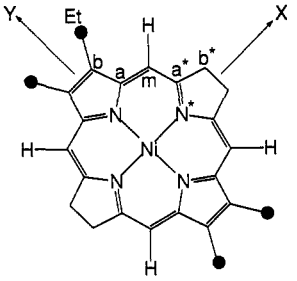

Figure 2. Structural diagram and labeling scheme for the model Ni(HOEBC) used in the normal mode analysis. The ethyl groups on the pyrrole rings are approximated as a point mass (15 amu) while all the substituents on the reduced rings are trucated to preserve D_{2h} symmetry. The asterisk indicates atoms of the pyrroline rings.

Table I. Structural Parameters Used in Normal Coordinate Analysis of Ni(HOEBC)[a]

	pyrrole rings	pyrroline rings
	Bond Length (Å)	
C_β–C_β	1.370	1.538
C_α–C_m	1.393	1.361
C_α–N	1.381	1.386
C_α–C_β	1.433	1.513
C_β–C_{Et}	1.502	1.513
Ni–N	1.940	1.930
C_m–H	1.095	
	Bond Angle (deg)	
C_α–N–C_α	102.9	103.3
C_α–C_β–C_β	106.0	102.1
N–C_α–C_β	112.5	116.2
C_α–C_m–C_α	123.6	
C_β–C_α–C_m	123.0	118.2
N–C_α–C_m	124.4	125.1
C_β–C_β–C_{Et}	126.0	
C_α–C_m–H	118.2	118.2
C_α–N–Ni	128.5	125.1
N–Ni–N	90	90

[a] The bond distances and valence bond angles were averaged from the crystal structure of nickel(II) octaethylbacteriochlorin (ref 22) with slight modification of bond angles to maintain a D_{2h} symmetry of the macrocycle.

of a β-substituted porphyrin (OEP),[20] a dihydroporphyrin (OEC),[12] and tetrahydroporphyrins (OEiBC[16] and OEBC), which is expected to provide a basis for detailed studies of the more complex hemes, sirohemes, chlorophylls, and bacteriochlorophylls.

Experimental Section

Synthesis of HOEBC and Its Derivatives. The free base of HOEBC was synthesized by using methyllithium to methylate 1,5-dioxooctaethylbacteriochlorin, which was prepared from octaethylporphyrin according to the method of Chang.[19b] Quantitative *meso* deuterium exchange was achieved by warming 5 mg of 1,5-dioxooctaethylbacteriochlorin in 1 mL of trifluoroacetic acid-d_1 at 100 °C for 2 h. No loss of *meso*-deuterium was found to accompany the methylation or metal insertion reaction, as monitored by NMR and RR spectra. Nickel was incorporated into free base HOEBC using a five-fold excess of $NiCl_2$, in boiling dimethylformamide (DMF). The dried solid was chromatographed on a preparative Silica plate (Analtech, Silica Gel G) with methylene chloride as eluent to remove trace amount of fluorescent fractions.

Spectroscopy. Resonance Raman spectra were obtained in backscattering geometry from either a methylene chloride solution in a spinning NMR tube or a rotating KBr pellet. Excitation lines were provided with a Coherent Innova 100K3 krypton ion laser (406.7, 530.9, and 676.4 nm) and a Spectra-Physics 2025 argon ion laser (488.0 nm). The scattered light was collected and dispersed with either a Spex 1404 double monochromator (for solid samples) or a Spex 1877 triplemate equipped with a Princeton Instruments cooled intensified diode array detection system (for solution samples). It was noticed in the initial trial experiments that Ni(HOEBC) complexes were gradually degraded in the presence of oxygen during prolonged laser illumination. Accordingly, the solution

(9) (a) Andersson, L. A.; Loehr, T. M.; Lim, A. R.; Mauk, A. G. *J. Biol. Chem.* **1984**, *259*, 15340. (b) Andersson, L. A.; Loehr, T. M.; Chang, C. K.; Mauk, A. G. *J. Am. Chem. Soc.* **1985**, *107*, 182. (c) Andersson, L. A.; Loehr, T. M.; Sotiriou, C.; Wu, W.; Chang, C. K. *J. Am. Chem. Soc.* **1986**, *108*, 2908. (d) Andersson, L. A.; Sotiriou, C.; Chang, C. K.; Loehr, T. M. *J. Am. Chem. Soc.* **1987**, *109*, 258. (e) Andersson, L. A.; Loehr, T. M.; Stershic, M. T.; Stolzenberg, A. M. *Inorg. Chem.* **1990**, *29*, 2278. (f) Andersson, L. A.; Loehr, T. M.; Thompson, R. G.; Strauss, S. H. *Inorg. Chem.* **1990**, *29*, 2142.

(10) (a) Ozaki, Y.; Kitagawa, T.; Ogoshi, H. *Inorg. Chem.* **1979**, *18*, 1772. (b) Ozaki, Y.; Iriyama, K.; Ogoshi, H.; Ochiai, T.; Kitagawa, T. *J. Phys. Chem.* **1986**, *90*, 6105.

(11) (a) Salehi, A.; Oertling, W. A.; Fonda, H. N.; Babcock, G. T.; Chang, C.K. *Photochem. Photobiol.* **1988**, *48*, 525–530. (b) Fonda, H. N.; Oertling, W. A.; Salehi, A.; Chang, C. K.; Babcock, G. T. *J. Am. Chem. Soc.* **1990**, *112*, 9497–9507.

(12) Prendergast, K.; Spiro, T. G. *J. Phys. Chem.* **1991**, *95*, 1555–1563.

(13) (a) Boldt, N. J.; Donohoe, R. J.; Birge, R. R.; Bocian, D. F. *J. Am. Chem. Soc.* **1987**, *109*, 2284. (b) Donohoe, R. J.; Atamian, M.; Bocian, D. F. *J. Phys. Chem.* **1989**, *93*, 2244. (c) Procyk, A. D.; Kim, Y.; Schmidt, E.; Fonda, H. N.; Chang, C. K.; Babcock, G. T.; Bocian, D. F. *J. Am. Chem.* **1992**, *114*, 6539–6549.

(14) Gladkov, L. L.; Starukhin, A. S.; Shulga, A. M. *Spectrochim. Acta* **1987**, *43A*, 1125.

(15) (a) Cotton, T. M.; Timkovich, R.; Cork, M. S. *FEBS Lett.* **1981**, *133*, 39–44. (b) Ching, Y.; Ondrias, M. R.; Rousseau, D. L.; Muhoberac, B. B.; Wharton, D. C. *FEBS Lett.* **1982**, *138*, 239–244. (c) Ondrias, M. R.; Carson, S. D.; Hirasawa, M.; Knaff, D. B. *Biochim. Biophys. Acta* **1985**, *830*, 159–163. (d) Han, S.; Madden, J. F.; Thompson, R. G.; Strauss, S. H.; Siegel, L. M.; Spiro, T. G. *Biochemistry* **1989**, *28*, 5461–5470. (e) Andersson, L. A.; Loehr, T. M.; Wu, W.; Chang, C. K.; Timkovich, R. *FEBS Lett.* **1990**, *267*, 285–288. (f) Andersson, L. A.; Loehr, T. M.; Thompson, R. G.; Strauss, S. H. *Inorg. Chem.* **1990**, *29*, 2142. (g) Lai, K. K.; Yue, K. T. *J. Raman Spectrosc.* **1990**, *21*, 21–26.

(16) Melamed, D.; Sullivan, E. P.; Prendergast, K.; Strauss, S. H.; Spiro, T. G. *Inorg. Chem.* **1991**, *30*, 1308–1319.

(17) Procyk, A. D.; Bocian, D. F. *J. Am. Chem. Soc.* **1991**, *113*, 3765–3773.

(18) (a) Eisner, U. *J. Chem. Soc.* **1957**, 3461–3469. (b) Whitlock, H. W.; Hanauer, R.; Oester, M. Y.; Bower, B. K. *J. Am. Chem. Soc.* **1969**, *91*, 7485–7489.

(19) (a) Inhoffen, H. H.; Nolte, W. *Justus Liebigs Ann. Chem.* **1969**, *725*, 167–176. (b) Chang, C. K. *Biochemistry* **1980**, *19*, 1971–1976.

(20) Li, X.-Y.; Czenuszewicz, R. S.; Kincaid, J. R.; Stein, P.; Spiro, T. G. *J. Phys. Chem.* **1990**, *94*, 47–61.

Table II. Valence Force Constants for Ni(HOEBC)

	pyrrole	pyrroline		pyrrole	pyrroline
		Stretch (mdyn/Å)			
$K(C_{Et}C_\beta)$	4.500		$K(C_\beta C_\beta)$	7.350	3.400
$K(C_\alpha C_\beta)$	5.650	4.400	$K(C_mH)$	5.020	
$K(C_\alpha C_m)$	6.600	7.600	K(NNi)	1.800	1.800
$K(C_\alpha N)$	5.600	5.700			
		Bend (mdyn/rad^2)			
$H(C_{Et}C_\beta C_\alpha)$	1.200		$H(C_\alpha NNi)$	0.300	0.300
$H(C_{Et}C_\beta C_\beta)$	1.200		$H(C_\beta C_\alpha C_m)$	0.830	0.830
$H(C_\alpha C_\beta C_\beta)$	1.370	0.900	$H(C_\beta C_\alpha N)$	1.370	0.900
$H(C_\alpha C_m C_\alpha)$	1.100		$H(C_m C_\alpha N)$	0.700	1.300
$H(C_\alpha C_m H)$	0.509	0.576	H(NNiN*)	0.250	
$H(C_\alpha NC_\alpha)$	1.620	1.620			
		1–2 Stretch–Stretch Interaction (mdyn/Å)			
$(C_\alpha C_\beta)(C_{Et}C_\beta)$	0.329		$(C_\beta C_\beta)(C_{Et}C_\beta)$	0.437	
$(C_\alpha C_m)(C_\alpha C_\beta)$	0.502	0.305	$(C_\beta C_\beta)(C_\alpha C_\beta)$	0.397	0.162
$(C_\alpha N)(C_\alpha C_\beta)$	0.442	0.348	$(C_\alpha C_m)(C_\alpha C_m)$	0.244	
$(C_\alpha N)(C_\alpha C_m)$	0.450	0.572	(NNi)$(C_\alpha N)$	0.480	0.458
$(C_\alpha N)(C_\alpha N)$	0.482	0.426	(NNi)(NNi)	0.165	
		Stretch–Bend Interaction (Sharing Two Atoms) (mdyn/rad)			
$(C_{Et}C_\beta)(C_{Et}C_\beta C_\alpha)$	0.383		$(C_\alpha C_m)(C_\beta C_\alpha C_m)$	0.305	0.345
$(C_{Et}C_\beta)(C_{Et}C_\beta C_\beta)$	0.319		$(C_\alpha C_m)(C_m C_\alpha N)$	0.261	0.261
$(C_\alpha C_\beta)(C_{Et}C_\beta C_\alpha)$	0.381		$(C_\alpha N)(C_\alpha NC_\alpha)$	0.214	0.219
$(C_\alpha C_\beta)(C_\alpha C_\beta C_\beta)$	0.323	0.166	$(C_\alpha N)(C_\alpha NNi)$	0.117	0.163
$(C_\alpha C_\beta)(C_\beta C_\alpha C_m)$	0.288	0.174	$(C_\alpha N)(C_\beta C_\alpha N)$	0.157	0.245
$(C_\alpha C_\beta)(C_\beta C_\alpha N)$	0.301	0.185	$(C_\alpha N)(C_m C_\alpha N)$	0.211	0.309
$(C_\alpha C_m)(C_\alpha C_m C_\alpha)$	0.277	0.360	$(C_\beta C_\beta)(C_{Et}C_\beta C_\beta)$	0.336	
$(C_\alpha C_m)(C_\alpha C_m H)$	0.124	0.167	$(C_\beta C_\beta)(C_\alpha C_\beta C_\beta)$	0.334	0.074
		Stretch–Bend Interaction (Sharing One Atom) (mdyn/rad)			
$(C_{Et}C_\beta)(C_\beta C_\alpha N)$	−0.239		$(C_\alpha C_m)(C_\alpha C_m H)$	−0.048	−0.128
$(C_\alpha C_\beta)(C_{Et}C_\beta C_\beta)$	−0.120		$(C_\alpha N)(C_\alpha C_m H)$	0.055	0.042
$(C_\alpha C_\beta)(C_\alpha NC_\alpha)$	−0.296	−0.114	$(C_\alpha N)(C_\beta C_\alpha C_m)$	−0.102	−0.248
$(C_\alpha C_\beta)(C_m C_\alpha N)$	−0.264	−0.290	$(C_\alpha N)(C_\beta C_\alpha N)$	−0.073	0.036
$(C_\alpha C_m)(C_\beta C_\alpha N)$	−0.246	−0.171	$(C_\alpha N)(C_m C_\alpha N)$	−0.280	−0.151
		1–3 Stretch–Stretch Interaction (mdyn/Å)			
$(C_\alpha C_\beta)(C_{Et}C_\beta)$	−0.250		$(C_\alpha N)(C_{Et}C_\beta)$	−0.250	
$(C_\alpha C_\beta)(C_\alpha C_\beta)$	0.250	0.200	$(C_\alpha N)(C_\beta C_\beta)$	0.250	0.200
$(C_\alpha C_\beta)(C_\alpha N)$	0.250	0.200	$(C_\alpha N)(C_\alpha C_m)$	−0.250	−0.250
$(C_\alpha C_m)(C_\alpha N)$	−0.200	−0.250	$(C_\alpha C_\beta)(C_\alpha C_m)$	−0.100	−0.250
$(C_\alpha C_m)(C_\beta C_\beta)$	−0.200		(NNi)$(C_\alpha C_\beta)$	−0.250	
		1–4 Stretch–Stretch Interaction (mdyn/Å)			
$(C_\alpha C_m)(C_\alpha C_m)$	−0.047	−0.077			

samples were vigorously degassed with at least three freeze–pump–thaw cycles, while the solid pellets were placed under vacuum.

The electronic absorption spectrum was obtained with a 1-cm quartz cell on a Hewlett-Packard 8452A diode array spectrophotometer. The FT-IR spectra of Ni(HOEBC) and its *meso*-d_4 isotopomer in KBr pellets were recorded on a Nicolet 730 Fourier transform infrared spectrophotometer. All the spectral data were imported into and processed with Labcalc software (Galactic Industries Corporation).

Normal Coordinate Analysis. Normal mode calculations were performed with the empirical GF matrix method of Wilson[21] and a valence force field adapted from those of NiOEP.[20] The molecular geometry was taken from the crystal structural data of nickel octaethylbacteriochlorin[22] and slightly modified to maintain D_{2h} symmetry. The internal coordinates consist of Wilson-type bond-stretching and angle-bending coordinates. The symmetry coordinates (S_i) and the corresponding U matrix were obtained from symmetry-adapted linear combination of internal coordinates. A menu-driven, graphically-interfaced version of Schachtschneider's programs,[23] developed in our laboratory and implemented on a R3000 Indigo workstation (Silicon Graphics Inc.), was used to set up the G matrix and to solve the secular equation $|\mathbf{GF} - \mathbf{E}\lambda| = 0$.

Results and Discussion

A. Normal Coordinate Analysis: Structure and Force Field. Figure 1 shows the molecular structure of bacteriochlorophyll a and of Ni(HOEBC). Ni(HOEBC) has the bacteriochlorin core structure and the β-substituent pattern of bacteriochlorophylls without the complication of the fifth isocyclic ring. Nickel rather than magnesium was chosen as the central metal, because the nickel complex gives fluorescence-free RR spectra throughout both the B and Q excitations. In addition, a high-quality force field for NiOEP[20] has been developed, accounting for almost all the in-plane skeletal vibrational modes, as well as the pyrrole-^{15}N, *meso*-d_4, and methylene-d_{16} isotope shifts.

To facilitate the spectral assignments, a normal mode analysis was performed on a model of Ni(HOEBC) having D_{2h} symmetry. In this model, shown in Figure 2, the ethyl groups on the pyrrole rings are approximated as point masses (15 amu), while the substituents on the pyrroline rings are eliminated to preserve the D_{2h} symmetry. These approximations are not expected to significantly affect the bacteriochlorin skeletal vibrations, inasmuch as the ethyl group vibrations are relatively independent of the other skeletal modes in the normal modes of NiOEP.[20] Table I gives the structural parameters for this idealized Ni(HOEBC) while Table II lists the valence force constants used in the calculation. The observed and calculated frequencies for natural abundance (N.A.)- and *meso*-d_4-Ni(HOEBC) are compared in Table III, along with their assignments and potential energy distributions. The calculated pyrrole and pyrroline ^{15}N isotope shifts are also included in Table III for future reference and for comparison with data on bacteriochlorophylls (see below).

Several crystal structures related to bacteriochlorophylls are available, including those of nickel octaethylbacteriochlorin,[22]

(21) Wilson, E. B.; Decius, J. C.; Cross, P. C. *Molecular Vibrations*; McGraw-Hill: New York, 1955.

(22) Waditschatka, R.; Kratky, C.; Jaun, B.; Heinzer, J.; Eschenmoser, A. *J. Chem. Soc., Chem. Commun.* **1985**, 1604–1607. The structural parameters were obtained from the Cambridge Structure Database.

(23) Schachtschneider, J. H. Technical Report Nos. 57–65 and 231–264, Shell Development Co., 1962.

Table III. Comparison of the Calculated and Observed Frequencies and Isotope Shifts for Ni(HOEBC)[a]

	obsd			calcd			
	mode	N.A.	$\Delta(d_4)$	N.A.	$\Delta(d_4)$	$\Delta(^{15}N)$	assignment (PED %)
A_g	1			3040	778	0	ν_1 $\nu(C_mH)(98)$
	2	1635	2	1638	11	0	ν_{10} $\nu(C^*_\alpha C_m)(48)$, $\nu(C_\alpha C_m)(31)$, $\delta(C^*_\alpha C_mH)(8)$, $\delta(C_\alpha C_mH)(6)$
	3	1583	2	1584	1	0	ν_2 $\nu(C_\beta C_\beta)(67)$, $\nu(C_{Et}C_\beta)(14)$, $\delta(C_{Et}C_\beta C_\alpha)(11)$, $\delta(C_\beta C_\alpha N)(8)$, $\nu(C_\alpha C_m)(8)$
	4	1467	21	1472	18	4	ν_3 $\nu(C^*_\alpha C_m)(27)$, $\nu(C_\alpha C_m)(20)$, $\nu(C_\alpha N)(16)$, $\nu(C^*_\alpha N^*)(11)$
	5	1396	17	1391	4	9	ν_4 $\nu(C^*_\alpha N^*)(31)$, $\nu(C_\alpha C_\beta)(20)$, $\nu(C^*_\alpha C^*_\beta)(19)$, $\delta(C_mC^*_\alpha N^*)(12)$, $\delta(C^*_\alpha N^*C^*_\alpha)(9)$
	6	1360	42	1357	36	5	ν_{12} $\nu(C_\alpha N)(29)$, $\delta(C_\alpha C_mH)(20)$, $\nu(C_\alpha C_\beta)(19)$, $\delta(C^*_\alpha C_mH)(16)$, $\nu(C^*_\alpha N^*)(8)$
	7	1284	344	1269	308	3	ν_{13} $\nu(C_\alpha C_\beta)(35)$, $\delta(C^*_\alpha C_mH)(16)$, $\delta(C_\alpha C_mH)(12)$, $\nu(C_{Et}C_\beta)(10)$, $\nu(C^*_\alpha C^*_\beta)(9)$
	8	1182	−40	1179	−34	15	ν_{14} $\delta(C_\alpha NC_\alpha)(14)$, $\nu(C_\alpha N)(13)$, $\nu(C_\alpha C_m)(9)$, $\nu(C_{Et}C_\beta)(9)$, $\delta(C^*_\alpha C_mH)(7)$
	9			1045	−19	0	ν_{11} $\nu(C^*_\beta C^*_\beta)(78)$, $\delta(C^*_\beta C^*_\alpha C_m)(7)$
	10	984	−5	983	−4	14	ν_6 $\nu(C^*_\alpha C^*_\beta)(51)$, $\nu(N^*Ni)(8)$, $\nu(C^*_\alpha N^*)(8)$
	11	764	16	776	6	7	ν_{15} $\nu(C_{Et}C_\beta)(38)$, $\delta(C_\alpha C_mC^*_\alpha)(11)$, $\nu(C_\alpha N)(10)$, $\nu(NNi)(9)$
	12	728	52	724	45	4	ν_{16} $\delta(C_\beta C_\alpha N)(13)$, $\delta(C_\alpha NC_\alpha)(9)$, $\nu(C_\alpha C_m)(8)$, $\delta(C_\alpha C_mC^*_\alpha)(6)$, $\nu(C_\alpha N)(6)$
	13	672	55	665	33	0	ν_7 $\nu(C^*_\alpha N^*)(19)$, $\nu(C_{Et}C_\beta)(11)$, $\delta(C^*_\beta C^*_\alpha N^*)(9)$, $\delta(C^*_\alpha N^*C^*_\alpha)(8)$, $\delta(C_\alpha C_mC^*_\alpha)(7)$
	14	381	2	377	1	1	ν_8 $\delta(C_{Et}C_\beta C_\beta)(19)$, $\delta(C_{Et}C_\beta C_\alpha)(16)$, $\nu(N^*Ni)(11)$, $\nu(C_\alpha C_\beta)(8)$, $\nu(C_\alpha C_m)(7)$
	15	340	1	329	0	1	ν_{17} $\delta(C_{Et}C_\beta C_\beta)(29)$, $\delta(C_{Et}C_\beta C_\alpha)(19)$, $\nu(N^*Ni)(16)$
	16			209	0	1	ν_{18} $\nu(NNi)(41)$, $\nu(N^*Ni)(21)$, $\delta(C_mC^*_\alpha N^*)(10)$, $\delta(C_mC_\alpha N)(9)$
B_{1g}	17			3040	780	0	ν_{27} $\nu(C_mH)(98)$
	18	1607	11	1608	13	0	ν_{19} $\nu(C^*_\alpha C_m)(47)$, $\nu(C_\alpha C_m)(39)$, $\delta(C^*_\alpha C_mH)(10)$, $\delta(C_\alpha C_mH)(7)$
	19	1489	4	1490	7	3	ν_{28} $\nu(C_\alpha C_\beta)(28)$, $\delta(C_\alpha C_\beta C_\beta)(22)$, $\nu(C_\alpha N)(20)$, $\nu(C_{Et}C_\beta)(18)$, $\delta(C_{Et}C_\beta C_\beta)(11)$
	20	1421	14	1416	10	4	ν_{29} $\nu(C_\alpha C_\beta)(25)$, $\nu(C^*_\alpha C_m)(21)$, $\nu(C_\alpha C_m)(20)$, $\nu(C^*_\alpha N^*)(17)$, $\nu(C_\alpha N)(8)$
	21	1340	450	1337	455	6	ν_{21} $\nu(C^*_\alpha N^*)(31)$, $\delta(C^*_\alpha C_mH)(21)$, $\delta(C_\alpha C_mH)(13)$, $\nu(C_\alpha N)(9)$, $\nu(C_\alpha C_\beta)(9)$
	22	1218	−72	1224	−65	3	ν_{20} $\nu(C^*_\alpha C^*_\beta)(41)$, $\nu(C^*_\alpha N^*)(15)$, $\delta(C_\alpha C_mH)(14)$, $\delta(C^*_\alpha C_mH)(6)$, $\nu(C_\alpha N)(6)$
	23	1129	−40	1138	−44	10	ν_{22} $\nu(C_\alpha N)(40)$, $\nu(C_{Et}C_\beta)(17)$, $\nu(C_\alpha C_\beta)(10)$, $\delta(C^*_\alpha C_mH)(9)$, $\nu(C^*_\alpha N^*)(8)$
	24	1060	−2	1061	−6	17	ν_{30} $\nu(C^*_\alpha N^*)(23)$, $\delta(C_mC^*_\alpha N^*)(14)$, $\nu(C^*_\alpha C^*_\beta)(13)$, $\delta(C_\alpha C_mC^*_\alpha)(9)$, $\nu(C^*_\alpha C_m)(8)$
	25	1020	−6	1023	2	5	ν_{23} $\nu(C_\alpha C_m)(19)$, $\nu(C_{Et}C_\beta)(13)$, $\nu(C^*_\alpha C^*_\beta)(11)$, $\nu(C_\alpha C_\beta)(8)$, $\delta(C_\alpha C_mC^*_\alpha)(6)$
	26	824	9	824	3	3	ν_{32} $\delta(C_{Et}C_\beta C_\beta)(16)$, $\delta(C_{Et}C_\beta C_\alpha)(14)$, $\delta(C^*_\alpha C^*_\beta C^*_\beta)(12)$, $\nu(C^*_\alpha C^*_\beta)(11)$, $\delta(C_mC_\alpha N)(9)$
	27	667	5	657	2	3	ν_{24} $\delta(C^*_\alpha C^*_\beta C^*_\beta)(25)$, $\delta(C_mC^*_\alpha N^*)(17)$, $\delta(C_{Et}C_\beta C_\alpha)(10)$, $\delta(C^*_\beta C^*_\alpha N^*)(6)$
	28	581	10	581	8	2	ν_{25} $\nu(C_{Et}C_\beta)(25)$, $\delta(C_\alpha C_\beta C_\beta)(14)$, $\delta(C^*_\alpha C^*_\beta C^*_\beta)(11)$, $\delta(C^*_\beta C^*_\alpha C_m)(10)$, $\delta(C^*_\beta C^*_\alpha N^*)(8)$
	29			440	3	1	ν_{33} $\delta(C^*_\beta C^*_\alpha C_m)(24)$, $\delta(C_mC^*_\alpha N^*)(12)$, $\delta(C_\alpha C_\beta C_\beta)(7)$, $\delta(C_{Et}C_\beta C_\alpha(7)$, $\nu(C_\alpha C_m)(7)$
	30	271[b]	2	260	2	1	ν_{26} $\delta(C_\beta C_\alpha C_m)(15)$, $\nu(C_\alpha C_\beta)(11)$, $\delta(C_{Et}C_\beta C_\beta)(9)$, $\delta(C_\alpha C_mC^*_\alpha)(7)$, $\delta(C_{Et}C_\beta C_\alpha)(7)$
	31			182	2	1	ν_{35} $\delta(C_\alpha NNi)(22)$, $\delta(NNiN^*)(18)$, $\delta(C^*_\alpha N^*Ni)(14)$, $\delta(C_\alpha C_mC^*_\alpha)(12)$, $\delta(C_\beta C_\alpha C_m)(8)$
B_{2u}	32			3040	779	0	ν_{36a} $\nu(C_mH)(98)$
	33	1610	12	1619	13	0	ν_{37a} $\nu(C^*_\alpha C_m)(41)$, $\nu(C_\alpha C_m)(35)$, $\delta(C^*_\alpha C_mH)(9)$, $\nu(C_\beta C_\beta)(9)$, $\delta(C_\alpha C_mH)(7)$
	34	1543[c]	1	1583	2	0	ν_{38a} $\nu(C_\beta C_\beta)(63)$, $\nu(C_{Et}C_\beta)(13)$, $\nu(C_\alpha C_m)(12)$, $\delta(C_{Et}C_\beta C_\alpha)(11)$, $\delta(C_\beta C_\alpha N)(8)$
	35			1447	13	5	ν_{39a} $\nu(C^*_\alpha C_m)(31)$, $\nu(C_\alpha N)(19)$, $\nu(C_\alpha C_m)(15)$, $\nu(C^*_\alpha N^*)(11)$
	36			1360	405	6	ν_{42a} $\nu(C_\alpha C_\beta)(28)$, $\nu(C_\alpha N)(26)$, $\delta(C_\alpha C_mH)(16)$, $\delta(C^*_\alpha C_mH)(11)$, $\nu(C^*_\alpha N^*)(11)$
	37			1334	−10	4	ν_{40a} $\nu(C_\alpha C_\beta)(35)$, $\nu(C^*_\alpha N^*)(28)$, $\delta(C^*_\alpha C_mH)(13)$, $\nu(C^*_\alpha C^*_\beta)(11)$
	38	1187		1198	−90	3	ν_{41a} $\nu(C^*_\alpha C^*_\beta)(43)$, $\nu(C^*_\alpha N^*)(16)$, $\delta(C_\alpha C_mH)(10)$, $\nu(C_\alpha C_\beta)(10)$, $\delta(C^*_\alpha C_mH)(9)$
	39			1184	−6	15	ν_{43a} $\delta(C_\alpha NC_\alpha)(13)$, $\nu(C_\alpha N)(9)$, $\delta(C^*_\alpha C_mH)(8)$, $\nu(C^*_\alpha N^*)(8)$, $\nu(C_\alpha C_m)(8)$
	40	1055	−2	1034	2	18	ν_{45a} $\nu(C^*_\alpha N^*)(23)$, $\nu(C^*_\alpha C^*_\beta)(18)$, $\delta(C_mC^*_\alpha N^*)(14)$, $\nu(C^*_\alpha C_m)(11)$, $\delta(C_\alpha C_mC^*_\alpha)(7)$
	41			807	15	2	ν_{46a} $\nu(C^*_\alpha C^*_\beta)(15)$, $\delta(C_\alpha C_mC^*_\alpha)(14)$, $\nu(C_{Et}C_\beta)(13)$, $\nu(C_\alpha N)(12)$, $\delta(C^*_\alpha C^*_\beta C^*_\beta)(10)$
	42	743	25	759	34	7	ν_{47a} $\nu(C_{Et}C_\beta)(33)$, $\nu(NNi)(14)$, $\delta(C_\beta C_\alpha N)(9)$, $\delta(C_\alpha NC_\alpha)(7)$
	43	670	16	647	15	0	ν_{48a} $\delta(C^*_\alpha C^*_\beta C^*_\beta)(37)$, $\delta(C^*_\beta C^*_\alpha N^*)(15)$
	44			405	2	1	ν_{49a} $\nu(NNi)(19)$, $\alpha(C^*_\beta C^*_\alpha C_m)(15)$, $\nu(C_\alpha C_m)(9)$, $\delta(C^*_\alpha N^*Ni)(8)$
	45			368	2	2	ν_{50a} $\delta(C_{Et}C_\beta C_\beta)(16)$, $\nu(NNi)(13)$, $\delta(C_mC^*_\alpha N^*)(10)$, $\delta(C_mC_\alpha N)(7)$, $\delta(C_\alpha C_mC^*_\alpha)(7)$
	46			333	0	0	ν_{51a} $\delta(C_{Et}C_\beta C_\beta)(26)$, $\delta(C_{Et}C_\beta C_\alpha)(26)$, $\nu(NNi)(26)$
	47			285	2	1	ν_{53a} $\delta(C_\beta C_\alpha C_m)(11)$, $\nu(NNi)(10)$, $\nu(C_\alpha C_m)(7)$, $\delta(NNiN^*)(6)$, $\delta(C^*_\alpha N^*Ni)(6)$
B_{3u}	48			3040	779	0	ν_{36b} $\nu(C_mH)(98)$
	49	1632	1	1631	11	0	ν_{37b} $\nu(C^*_\alpha C_m)(53)$, $\nu(C_\alpha C_m)(30)$, $\delta(C^*_\alpha C_mH)(8)$, $\delta(C_\alpha C_mH)(6)$
	50	1516	9	1494	6	4	ν_{39b} $\nu(C_\alpha N)(23)$, $\nu(C_\alpha C_\beta)(22)$, $\delta(C_\alpha C_\beta C_\beta)(21)$, $\nu(C_{Et}C_\beta)(17)$, $\delta(C_{Et}C_\beta C_\beta)(10)$
	51	1420	21	1435	19	2	ν_{40b} $\nu(C_\alpha C_\beta)(26)$, $\nu(C_\alpha C_m)(20)$, $\nu(C^*_\alpha N^*)(17)$, $\nu(C^*_\alpha C_m)(17)$, $\delta(C_{Et}C_\beta C_\beta)(7)$
	52	1375	30	1382	6	11	ν_{41b} $\nu(C^*_\alpha N^*)(34)$, $\nu(C^*_\alpha C^*_\beta)(18)$, $\nu(C_\alpha C_m)(12)$, $\delta(C_mC^*_\alpha N^*)(11)$, $\nu(C_\alpha C_\beta)(10)$
	53			1300	391	4	ν_{42b} $\delta(C_\alpha C_mH)(28)$, $\delta(C^*_\alpha C_mH)(25)$, $\nu(C_\alpha N)(11)$, $\nu(C^*_\alpha C^*_\beta)(8)$
	54	1153	−15	1143	−55	10	ν_{44b} $\nu(C_\alpha N)(45)$, $\nu(C_{Et}C_\beta)(21)$, $\nu(C_\alpha C_\beta)(11)$, $\delta(C^*_\alpha C_mH)(6)$
	55	1066	−10	1077	−26	2	ν_{38b} $\nu(C^*_\beta C^*_\beta)(44)$, $\delta(C^*_\beta C^*_\alpha C_m)(6)$, $\nu(C_{Et}C_\beta)(6)$
	56			1006	−8	4	ν_{43b} $\nu(C^*_\alpha C^*_\beta)(29)$, $\nu(C^*_\beta C^*_\beta)(23)$, $\nu(C_{Et}C_\beta)(7)$
	57	976	−1	971	−3	14	ν_{46b} $\nu(C^*_\beta C^*_\beta)(15)$, $\nu(C^*_\alpha C^*_\beta)(13)$, $\nu(C_\alpha C_m)(12)$, $\nu(C^*_\alpha N^*)(9)$, $\delta(C_\alpha C_mC^*_\alpha)(8)$
	58			845	25	3	ν_{47b} $\delta(C_mC_\alpha N)(15)$, $\delta(C_{Et}C_\beta C_\beta)(14)$, $\delta(C_{Et}C_\beta C_\alpha)(13)$, $\delta(C_\beta C_\alpha C_m)(12)$, $\nu(C^*_\alpha C^*_\beta)(12)$
	59			628	24	1	ν_{48b} $\nu(C^*_\alpha N^*)(16)$, $\delta(C_{Et}C_\beta C_\beta)(10)$, $\nu(C^*_\alpha N^*C^*_\alpha)(9)$, $\delta(C^*_\beta C^*_\alpha N^*)(8)$, $\nu(C^*_\alpha C_m)(7)$
	60	585	8	577	6	4	ν_{49b} $\nu(C_{Et}C_\beta)(25)$, $\delta(C_\alpha C_\beta C_\beta)(16)$, $\delta(C_{Et}C_\beta C_\alpha)(16)$, $\delta(C_\alpha C_mC^*_\alpha)(7)$
	61			425	0	1	ν_{50b} $\nu(N^*Ni)(54)$, $\delta(C_mC^*_\alpha N^*)(6)$
	62	308[d]	1	302	3	1	ν_{52b} $\delta(C_\alpha NNi)(16)$, $\nu(N^*Ni)(13)$, $\delta(C^*_\beta C^*_\alpha C_m)(10)$, $\delta(NNiN^*)(9)$, $\delta(C^*_\alpha N^*C^*_\alpha)(6)$
	63			177	0	0	ν_{53b} $\delta(C_\beta C_\alpha C_m)(21)$, $\delta(C_mC_\alpha N)(9)$, $\delta(C_{Et}C_\beta C_\beta)(8)$, $\nu(C^*_\alpha C_m)(8)$, $\delta(C_{Et}C_\beta C_\alpha)(7)$

[a] The asterisk indicates atoms located on the pyrroline rings. [b] Observed only in the 530.9-nm excitation RR spectrum (not shown). [c] This band is weak in the IR spectrum but is clearly observed in the RR spectrum. [d] Observed in the 488.0-nm excitation RR spectrum.

zinc tetraphenylbacteriochlorin,[24] and several bacteriochlorin free bases.[25] They help reveal the essential structural characteristics of this class of tetrahydroporphyrins. As expected from the reduction of pyrrole rings, the pyrroline rings have much longer C_β–C_β and C_α–C_β bonds than do the pyrrole rings. In addition, the C_α–C_m bond length adjacent to the reduced rings is significantly shorter (0.04 Å on average) than those adjacent to pyrrole rings. This notable feature is also apparent in the crystal

(24) Barkigia, K. M.; Miura, M.; Thompson, M. A.; Fajer, J. *Inorg. Chem.* **1991**, *30*, 2233–2236.

(25) (a) Barkigia, K. M.; Fajer, J.; Smith, K. M.; Williams, G. J. B. *J. Am. Chem. Soc.* **1981**, *103*, 5890–5893. (b) Barkigia, K. M.; Fajer, J.; Chang, C. K.; Young, R. *J. Am. Chem. Soc.* **1984**, *106*, 6457–6459. (c) Barkigia, K. M.; Gottfield, D. S.; Boxer, S. G.; Fajer, J. *J. Am. Chem. Soc.* **1989**, *111*, 6444–6446.

(26) (a) Strauss, S. H.; Silver, M. E.; Long, K. M.; Thompson, R. G.; Hudgens, R. A.; Spartalian, K.; Ibers, J. A. *J. Am. Chem. Soc.* **1985**, *107*, 4207–4215. (b) Stolzenberg, A. M.; Schussel, L. J.; Summers, J. S.; Foxman, B. M.; Petersen, J. L. *Inorg. Chem.* **1992**, *31*, 1678–1686. (c) Barkigia, K. M.; Thompson, M. A.; Fajer, J. *New. J. Chem.* **1992**, *16*, 599–607.

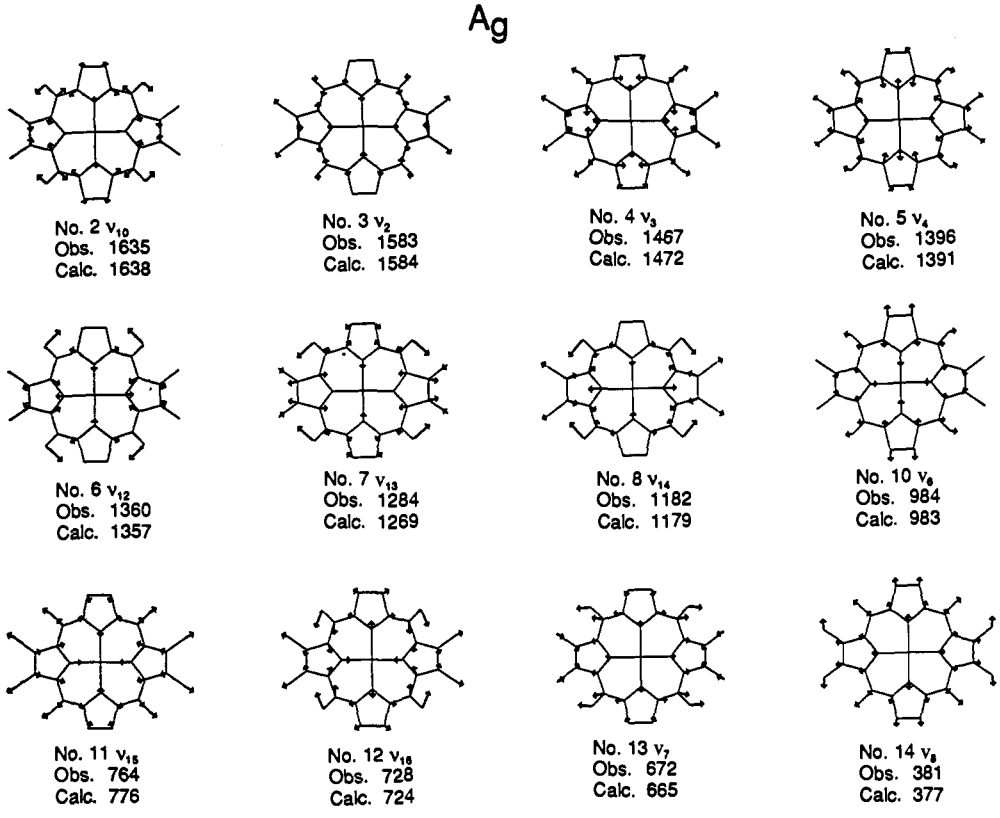

Figure 3. Vibrational eigenvectors for the high-frequency and some selected low-frequency A_g modes of Ni(HOEBC).

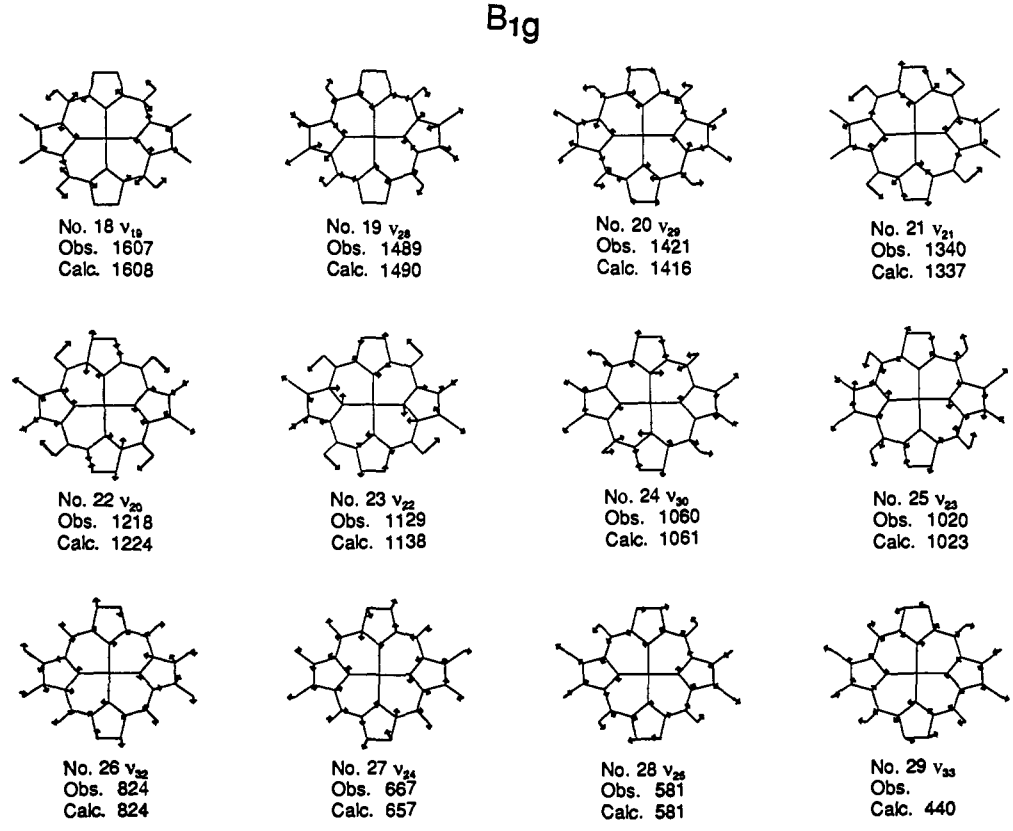

Figure 4. Same as Figure 3, but for B_{1g} modes.

structures of metallochlorins[26] and metalloisobacteriochlorins.[27] The crystal structure of Ni(OEBC) shows severe out-of-plane distortion of the macrocycle. A planar molecule was used in our calculation, however, to avoid the combination of both the in-plane and out-of-plane force field and to keep the calculated frequencies tractable under the D_{2h} symmetry. It is known that ruffling of NiOEP changes the frequencies of some skeletal vibrations but does not alter the mode characters, as judged from

(27) Suh, M. P.; Swepston, P. N.; Ibers, J. A. *J. Am. Chem. Soc.* **1984**, *106*, 5164.

(28) Czernuszewicz, R. S.; Li, X.-Y.; Spiro, T. G. *J. Am. Chem. Soc.* **1989**, *111*, 7024–7031.

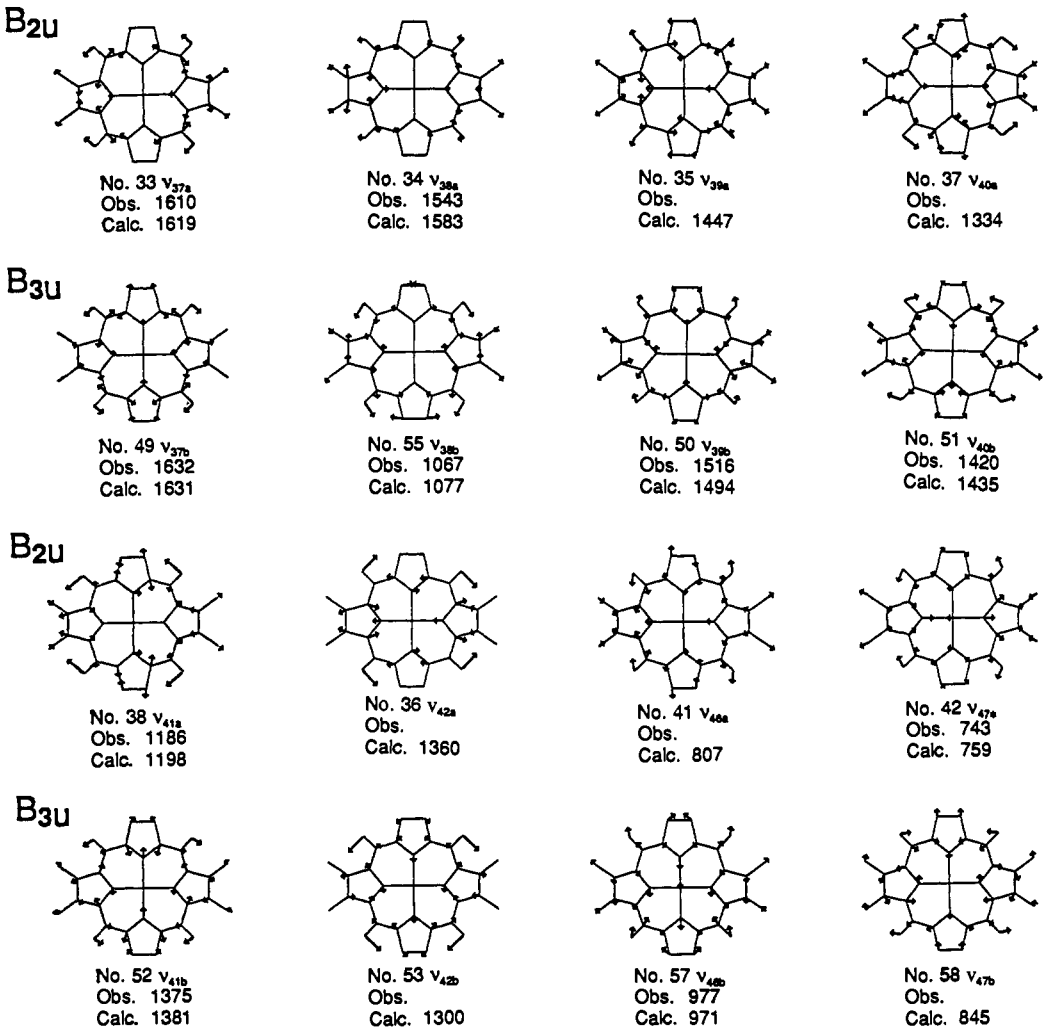

Figure 5. Comparison of the vibrational eigenvectors for some selected B_{2u} and B_{3u} modes, showing the splitting of E_u modes.

their isotope shifts.[28] Thus the planar model should serve as an adequate guide to in-plane mode assignments, even if the frequencies may not be accurate.

The general valence force field developed for NiOEP[20] was used to initiate the calculation. As in the case of NiOEC[12] and NiOEiBC,[16] the C–C and C–N stretching force constants were first scaled to their bond distances, using the equation of Burgi–Dunitz.[29] The associated 1,2 stretch–stretch interaction and valence angle bending force constants were also proportionally adjusted. These force constants were then slightly changed to improve the fit after the other interaction terms had been allowed into the least-square refinement regression. We adopted this approach because the bond stretch and related force constants can be more reliably rationalized than the bending terms. The final force field, listed in Table II, reproduced 50 observed RR frequencies for N.A.- and *meso*-d_4-Ni(HOEBC) with an average error of 6.2 cm^{-1} for each molecule. Although the calculation, to a large extent, satisfactorily accounts for the observed frequencies, the force field is open to further improvement, since relatively few observed frequencies are included in the calculation. More experimental data of other isotope frequencies, particularly those of the pyrrole ^{15}N-labeled Ni(HOEBC), will be helpful.

We note that two additional cross-ring 1,4 C_α–C_m stretch–stretch interaction force constants were introduced in our calculation, namely for the two C_α–C_m bonds adjacent to each pyrrole and pyrroline ring. These terms had not been included in the force field of NiOEP[20] but are needed to narrow the frequency difference between the ν_{10} and ν_{19} modes, which are separated by only 28 cm^{-1} for Ni(HOEBC) but by more than 50 cm^{-1} for NiOEP. The inclusion of these two terms saves major modification of other related force constants to yield a reasonable fit of the observed and calculated frequencies.

The calculated vibrational modes, given in Table III, are conventionally classified into A_g, B_{1g}, B_{2u}, and B_{3u} symmetries; the modes within each symmetry block are listed in descending order of frequencies. The mode labeling developed for NiOEP is adapted to Ni(HOEBC) to facilitate comparisons, although the mode compositions differ somewhat. This difference is reflected, for example, in enhanced *meso*-d_4 sensitivity of some of the Ni(HOEBC) modes which correlate with the a_{1g} modes of NiOEP, because of contributions from $\delta(C_mH)$. Such contributions to a_{1g} modes are forbidden under D_{4h} symmetry. Figures 3–5 give plots of the calculated vibrational eigenvectors for some selected modes of Ni(HOEBC). Table IV categorizes the observed frequencies (or the calculated ones in the absence of the experimental values) on the basis of their local coordinates, along with those of NiOEP for the purpose of comparison. It should be noted that our truncated model for Ni(HOEBC) eliminates half of the vibrations involving C_β–C_1 coordinates in NiOEP: ν_5, ν_9, ν_{31}, ν_{34}, ν_{45b}, and ν_{52a}.

B. RR Enhancement Pattern. Figure 6 shows how the relative intensity of RR bands varies at four different excitation lines at 406.7, 488.0, 530.9, and 676.4 nm, whose relationship to the electronic absorption spectrum is shown in Figure 7. The visible electronic transitions can be explained on the basis of Gouterman's four-orbital model for a D_{4h} metalloporphyrin, adapted and diagrammed in Figure 8 for a D_{2h} metallobacteriochlorin.[30] The D_{4h} symmetry labels of the HOMO and LUMO orbitals for

(29) Burgi, H.; Dunitz, J. D. *J. Am. Chem. Soc.* **1987**, *109*, 2924–2927.

(30) Gouterman, M. *J. Mol. Spectrosc.* **1961**, *6*, 138–161.

Table IV. Allocation of the Observed Frequencies for Ni(HOEBC) to the Local Coordinates[a]

		A_g		B_{1g}			
local coordinate	symmetry	A_{1g}	B_{1g}	A_{2g}	B_{2g}	B_{2u} (a) E_u	B_{3u} (b)
$\nu(C_mH)$	D_{2h}	[3040]			[3040]	[3040]	[3040]
	D_{4h}	ν_1 [3041]			ν_{27} [3041]	ν_{36} [3040]	
$\nu(C_\alpha C_m)_{asym}$	D_{2h}		1635	1607		1610	1632
	D_{4h}		ν_{10} 1655	ν_{19} 1603		ν_{37} [1637]	
$\nu(C_\beta C_\beta)$	D_{2h}	1583	[1045]			1543	1066
	D_{4h}	ν_2 1602	ν_{11} 1577			ν_{38} 1604	
$\nu(C_\alpha C_m)_{sym}$	D_{2h}	1467			1489	[1447]	1516
	D_{4h}	ν_3 1520			ν_{28} 1483	ν_{39} 1501	
ν(pyr quarter-ring)	D_{2h}			1218	1421	[1334]	1420
	D_{4h}			ν_{20} 1393	ν_{29} 1407	ν_{40} 1396	
$\nu(\text{pyr half-ring})_{sym}$	D_{2h}	1396	1360			1187	1375
	D_{4h}	ν_4 1384	ν_{12} 1343			ν_{41} [1346]	
$\delta(C_mH)$	D_{2h}		1284	1340		[1360]	[1300]
	D_{4h}		ν_{13} 1220	ν_{21} 1307		ν_{42} 1231	
$\nu(C_\beta C_1)_{sym}$	D_{2h}		1182				1153
	D_{4h}	ν_5 1138	ν_{14} 1131			ν_{44} 1153	
$\nu(\text{pyr half-ring})_{asym}$	D_{2h}			1129	1060	[1184]	[1006]
	D_{4h}			ν_{22} 1121	ν_{30} 1159	ν_{43} 1133	
$\nu(C_\beta C_1)_{asym}$	D_{2h}			1020		1055	
	D_{4h}			ν_{23} 1058	ν_{31} 1015	ν_{45} 996	
$\delta(\text{pyr deform})_{asym}$	D_{2h}			667	824	[807]	976
	D_{4h}			ν_{24} 597	ν_{32} 938	ν_{46} 927	
ν(pyr breathing)	D_{2h}	984	764			743	[845]
	D_{4h}	ν_6 804	ν_{15} 751			ν_{47} 766	
$\delta(\text{pyr deform})_{sym}$	D_{2h}	672	728			670	[628]
	D_{4h}	ν_7 674	ν_{16} 746			ν_{48} 605	
δ(pyr rot.)	D_{2h}			581	[440]	[405]	585
	D_{4h}			ν_{25} 551	ν_{33} 493	ν_{49} 544	
ν(Ni–N)	D_{2h}	381	[209]			[368]	[425]
	D_{4h}	ν_8 361/343	ν_{18} 168			ν_{50} [358]	
$\delta(C_\beta\text{–}C_1)_{asym}$	D_{2h}					[333]	
	D_{4h}					ν_{51} 328	
$\delta(C_\beta C_1)_{sym}$	D_{2h}		340	271			308
	D_{4h}	ν_9 263/274	ν_{17} 305	ν_{26} [243]	ν_{34} 197	ν_{52} 263	
δ(pyr transl)	D_{2h}				[182]	[285]	[177]
	D_{4h}				ν_{35} 144	ν_{53} 212	

[a] The values following the assigment are those of NiOEP (ref 20). The bracketed values are the calculated frequencies, for which the experimental values are not available.

metalloporphyrins are retained for clarity. The $D_{4h} \rightarrow D_{2h}$ correlations are A_{1g}, $B_{1g} \rightarrow A_g$; A_{2g}, $B_{2g} \rightarrow B_{1g}$; and $E_u \rightarrow B_{2u}(x)$, $B_{3u}(y)$.

The reduction of two pyrroles in Ni(HOEBC) splits the degenerate e_g orbitals into x and y components and selectively raises the energy of the a_{1u} orbital, since it is concentrated on the pyrrole C_α and C_β atoms, while the a_{2u} orbital is concentrated on the C_m and N atoms. Consequently, the two y-polarized electronic transitions ($A_{1u}xB_{2g} = B_{2u}$ and $B_{1u}xB_{3g} = B_{2u}$ under D_{2h} symmetry) are energetically well separated, giving rise to the lowest (Q_y) and highest (B_y) energy absorption bands with nearly equal intensity. However, the two x-polarized transitions ($B_{1u}xB_{2g} = B_{3u}$ and $A_{1u}xB_{3g} = B_{3u}$) are nearly degenerate, and having same symmetry, they experience a large configuration interaction. The result is an intense B_x transition and a weak Q_x transition.[30] As in porphyrins, the $Q_x(0,1)$ vibronic sideband retains about 10% of the intensity of the B_x band through Q/B vibronic coupling.[31]

In metalloporphyrin RR spectroscopy,[5c,e] excitation into the Soret bands enhances predominantly the totally symmetric A_{1g} modes through the Franck–Condon (A term) scattering mechanism while excitation near the Q bands enhances mainly the nontotally symmetric modes through the vibronic (B term) scattering mechanism. For metallobacteriochlorin, similar enhancement patterns are expected for excitation in the region of the B_x and Q_x transitions, and they are indeed observed in the RR spectra. Thus, the A_g modes, ν_{10}, ν_{12}, and ν_{14} dominate the spectrum obtained with 406.7-nm (B_x) excitation. Interestingly, the A_g modes deriving from the porphyrin B_{1g} modes are stronger than those deriving from the A_{1g} modes, e.g., ν_2, ν_3, and ν_4, reflecting the strength of the symmetry reduction. As the excitation is tuned toward the Q_x transitions (488.0 and 530.9 nm), the B_{1g} modes, ν_{19} and ν_{21}, gain intensity and become dominant with 530.9-nm excitation, in resonance with Q_{x0}. It is interesting that these two modes derive from the porphyrin A_{2g} modes, which have rotational symmetry; the B_{1g} modes deriving from porphyrin B_{2g} modes, e.g., ν_{28} and ν_{29}, are not enhanced in resonance with the Q_x transitions and are apparently not effective in mixing the Q_x and B_x transitions. On the other hand, one of the A_g modes, ν_{14} (1182 cm^{-1}), gains substantial intensity at 530.9 nm. This mode derives from a porphyrin B_{1g} mode and apparently retains vibronic activity despite becoming totally symmetric in the D_{2h} point group.

An altered enhancement pattern is seen upon excitation at 676.4 nm, near resonance with the strong Q_y transition. Totally symmetric modes once again dominate the spectrum, as expected, but they are different from those that dominate the B_x resonant spectra. In particular, ν_{10}, the strongest band in the 406.7-nm-excited spectrum, is not detectable at 676.4 nm, while ν_2, which has only moderate enhancement at 406.7 nm, becomes one of the strongest bands at 676.4 nm. These changes reflect different shapes of the B_x and Q_y excited states, resulting in different relative displacments of the normal modes.

We note the relatively strong enhancement of several nontotally symmetric B_{1g} modes with B_x (406.7-nm) excitation: ν_{19}, ν_{20}, ν_{22}, ν_{28}, and ν_{29}. Their activity is attributed to vibronic mixing of B_x and the nearby B_y state. This mixing is related to the Jahn–Teller effect[32] in metalloporphyrins, for which B_x and B_y are degenerate. Intrastate coupling via the Jahn–Teller effect is believed to account for significant enhancement of activity of nontotally symmetric modes in the B-state-resonant spectra of metalloporphyrins.

(31) Sekino, H.; Kobayashi, H. *J. Chem. Phys.* **1987**, *86*, 5045.

(32) Shelnut, J. A.; Cheung, L. D.; Cheng, C. C.; Yu, N.-T.; Felton, R. H. *J. Chem. Phys.* **1977**, *66*, 3387.

Table V. Comparison of the Experimental Frequencies of NiOEP, NiOEC, NiOEiBC, and Ni(HOEBC)[a]

local coordinate	A_{1g}	B_{1g}	A_{2g}	B_{2g}	E_u	local coordinate	A_{1g}	B_{1g}	A_{2g}	B_{2g}	E_u
$\nu(C_mH)$	ν_1 [3041]			ν_{27} [3041]	ν_{36} [3040]	δ(pyr deform)$_{asym}$			ν_{24} 597	ν_{32} 938	ν_{46} 927
$\nu(C_\alpha C_m)_{asym}$		ν_{10} 1655	ν_{19} 1603		ν_{37} [1637]	1			[669]	[891]	926/[885]
1. NiOEC		1648	1590		1614/1608	2			692	905	960/921
2. NiOEiBC		1656	1531		1627/1619	3			667	824	[807]/976
3. Ni(HOEBC)		1635	1607		1610/1632	ν(pyr breathing)	ν_6 804	ν_{15} 751			ν_{47} 766
$\nu(C_\beta C_\beta)$	ν_2 1602	ν_{11} 1577			ν_{38} 1604	1	798	778			[794]/[808]
1	1588	1546			1572/[1114]	2	811	825			792/[762]
2	1594	1568			1145/1175	3	984	764			743/[845]
3	1583	[1045]			1543/1066	δ(pyr deform)$_{sym}$	ν_7 674	ν_{16} 746			ν_{48} 605
$\nu(C_\alpha C_m)_{sym}$	ν_3 1520			ν_{28} 1483	ν_{39} 1501	1	681	746			[623]/[630]
1	1512			1478	1482/[1491]	2	680	737			[691]/[683]
2	1508			1488	1553/1515	3	672	728			670/[628]
3	1467			1489	[1447]/1516	δ(pyr rot.)			ν_{25} 551	ν_{33} 493	ν_{49} 544
ν(pyr quarter-ring)			ν_{20} 1393	ν_{29} 1407	ν_{40} 1396	1			[610]	[434]	[565]/[579]
1			1392	1402	1382/[1403]	2			521	469	[528]/[518]
2			[1410]	1405	[1447]/[1443]	3			581	[440]	[405]/585
3			1218	1421	[1334]/1420	ν(Ni–N)	ν_8 360/343	ν_{18} 168			ν_{50} [358]
ν(pyr half-ring)$_{sym}$	ν_4 1383	ν_{12} 1343			ν_{41} [1346]	1	362/342	[172]			[381]/[386]
1	1367	[1300]			1349/[1355]	2	346/361	[197]			[405]/[403]
2	1386	1335			1394/[1402]	3	381	[209]			[368]/[425]
3	1396	1360			1187/1375	$\delta(C_\beta C_1)_{asym}$			[253]	ν_{34} 197	ν_{51} 328
$\delta(C_mH)$		ν_{13} 1220	ν_{21} 1307		ν_{42} 1231	1			[253]	[183]	[297]/[308]
1		1232	1308		1257/1252	2			244	202	[335]/[333]
2		1226	1306		1258/1235	3			271		[333]/
3		1284	1340		[1360]/[1300]	$\delta(C_\beta C_1)_{sym}$	ν_9 263/274	ν_{17} 305			ν_{52} 263
$\nu(C_\beta C_1)_{sym}$	ν_5 1138	ν_{14} 1131			ν_{44} 1153	1	[264]	[343]			[273]/[269]
1	1146	1204			[1103]/[1117]	2	299/281	[270]			[201]/[202]
2	1119	1154			[1115]/[1115]	3		340			/308
3		1182			/1153	δ(pyr transl)				ν_{35} 144	ν_{53} 212
ν(pyr half-ring)$_{asym}$			ν_{22} 1121	ν_{30} 1159	ν_{43} 1133	1				[150]	[160]/[157]
1			1124	1152	1127/1155	2				[158]	[117]/[130]
2			[1100]	1186	1208/[1195]	3				[182]	[285]/[177]
3			1129	1060	[1184]/[1006]						
$\nu(C_\beta C_1)_{asym}$			ν_{23} 1058	ν_{31} 1015	ν_{45} 996						
1			1026	[1004]	[1003]/[984]						
2			1060	[1037]	994/[1047]						
3			1020		1055/						

[a] For each local coordinate, the first row is the observed frequencies of NiOEP, along with the assignments; the other three rows are labeled 1, 2, and 3 for those of NiOEc, NiOEiBC, and Ni(HOEBC), respectively. The bracketed values are the calculated frequencies, for which experimental values are not available. Data for NiOEP, NiOEC, and NiOEiBC were taken from refs 20, 12, and 16, respectively.

There are two apparent violations of the selection rule for D_{2h} symmetry in the RR spectra, namely, the observation of bands at 1541 and 1518 cm^{-1}, which are assigned to ν_{38a} (B_{2u}) and ν_{39b} (B_{3u}). These two modes are IR allowed but Raman forbidden. The absence of *meso*-d_4 sensitivity of the 1541-cm^{-1} band leaves little ambiguity over its assignment to the B_{2u} C_β–C_β stretching mode (ν_{38a}). Surprisingly, this band does not seem to appear in the IR spectrum. On the other hand, the 1518-cm^{-1} RR band is seen in the IR spectrum at 1516 cm^{-1} with the same *meso*-d_4 shift (9 cm^{-1}). The observation of IR-active modes in the RR spectrum is attributed to the out-of-plane distortion of the macrocycle, which lowers the effective symmetry of the π electrons from D_{2h} and destroys the symmetry center.

C. Spectral Assignments. Figures 9 and 10 compare the high-frequency (900–1700-cm^{-1}) RR spectra obtained with 406.7- and 488.0-nm excitation for Ni(HOEBC) and its *meso*-d_4 isotopomer. The dotted lines correlate the modes and indicate the *meso*-d_4 isotope shifts. Low-frequency spectra are shown in Figures 11 and 12. The band labels are from those developed for the parent NiOEP.[20] The spectra were obtained on solid samples, which magnify the intensity of some bands in the middle-frequency region. Spectra obtained in methylene chloride solution are shown in Figure 13. Figure 14 displays the infrared spectra of Ni(HOEBC) and its *meso*-d_4 analogue.

The isotope shifts, selective enhancement patterns, and correspondence with NiOEP frequencies were used to assign the observed bands to the calculated modes. These assignments are detailed in Table III, while Table IV compares corresponding frequencies with NiOEP. The correspondence is quite close when account is taken of the expected effects of C_β–C_β bond reduction on two opposite pyrroles. Thus, only two C_β–C_β stretches remain in the ~1580-cm^{-1} region, a symmetric and an antisymmetric combination. The latter is assigned to ν_{38b}, since the unreduced C_β–C_β bonds are on the y axis of the molecule, while the former could be assigned to either ν_2 or ν_{11} (both of which involve in-phase stretching of trans C_β–C_β bonds in NiOEP); ν_2 is chosen arbitrarily. The two other C_β–C_β modes, ν_{11} and ν_{38b}, are calculated at ca. 1050 cm^{-1}, in the single-bond region; no suitable candidate bands have been located in the RR or IR spectra. Also attributable to ring reduction is the frequency lowering of one of the pyrrole quarter-ring stretching modes, ν_{20} and ν_{29} (the choice is again arbitrary in the D_{2h} point group), to 1218 cm^{-1}, from ~1400 cm^{-1}. In this case, both Raman bands are observed. Interestingly, however, the pyrrole half-ring stretches ν_4 and ν_{12} are unaffected by ring reductions, occurring at essentially the same frequencies as in NiOEP. These modes involve out-of-phase stretching of the C_α–C_β and C_α–N bonds. The two pyrrole breathing Raman bands, ν_6 and ν_{15}, are both at ~800 cm^{-1} in NiOEP, but one of them is raised to nearly 1000 cm^{-1} in Ni(HOEBC).

The eight C_α–C_m modes are at nearly the same frequencies for NiOEP and Ni(HOEBC), ~1600 cm^{-1} for the asymmetric stretches, ν_{10}, ν_{19}, $\nu_{37a,b}$, and ~1500 cm^{-1} for the symmetric stretches, ν_3, ν_{28} and $\nu_{39a,b}$. Some differences are observed, of course, e.g., the 20- and 50-cm^{-1} lowering of ν_{10} and ν_3, which may be due to the $C_\alpha C_m$ bond alterations in Ni(HOEBC). Also ν_3 is correctly calculated to be more sensitive to *meso*-d_4 deuteration in Ni(HOEBC) than in NiOEP (21 vs 7 cm^{-1}) because of mixing in of C_m–H bending character; this mixing is symmetry forbidden in D_{4h} but allowed in D_{2h}.

The in-plane C_m–H bending coordinate is extensively distributed among a number of modes in the spectral region between 1100 and 1400 cm^{-1}, inducing complex isotope shift patterns. An interesting aspect of this pattern is the phenomenon of deuteration-induced upshifts, via mode crossing. Two modes composed mainly of C_m–H bending are found at 1340 (ν_{21}) and 1284 (ν_{13}) cm^{-1};

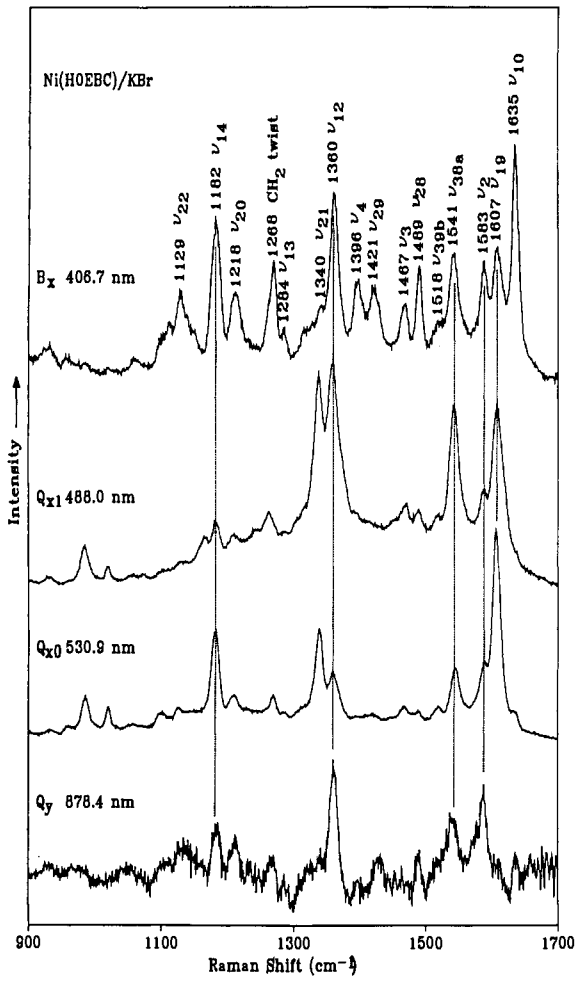

Figure 6. Resonance Raman spectra of Ni(HOEBC) in KBr pellet with variable excitation wavelengths, showing the intensity enhancement pattern. Major bands are labeled with frequencies and NiOEP-derived mode assignments. Experimental conditions: 1 cm^{-1}/ls, 2 scans, 4-cm^{-1} spectral slit, 20 mW for 406.7 nm, 50 mW for 488.0 and 530.9 nm, and 100 mW for 676.4 nm.

Table VI. Vibrational Assignments of Resonance Raman Frequencies of Bacteriochlorophyll a (BChl a) and Copper Bacteriopheophytin a (Cu(BPheo a))

BChl a ($\Delta^{15}N$)[a]	Cu(BPheo a)[b]	Ni(HOEBC) ($\Delta^{15}N$)[c]	assignment[d]
1695			ν(C=O)
1655			ν(C=O)
1605 (0)	1643	1635 (0)	ν_{10}
1537 (0)	1575	1583 (0)	ν_2
1525 (5)	1558	1508 (4)	ν_{39b}
1500 (2)	1511	1489 (3)	ν_{28}
1470 (1)	1484	1467 (4)	ν_3
1447 (0)	1460	1420 (2)	ν_{40}
1420 (4)	1433	1421 (4)	ν_{29}
1395 sh	1398		
1382 (3)	1380	1396 (9)	ν_4
1363 (10)	1362	1375 (11)	ν_{41b}
1345 (4)	1348	1340 (6)	ν_{21}
1289 (11)	1281	1284 (3)	ν_{13}
1257 (8)	1255	1300 (4)	ν_{42b}
1248 sh (5)			
1215 (4)	1232	1218 (3)	ν_{20}
1205 (0)		1186 (3)	ν_{41a}
1165 (8)	1151	1182 (15)	ν_{14}
1144 (14)		1154 (10)	ν_{44b}
1120 (10)		1129 (10)	ν_{22}

[a] Taken from Lutz, ref 5a. [b] Taken from Donohoe et al., ref 7h. [c] This work. The ^{15}N shifts are the calculated ones from Table III. [d] The nomenclature for the assignments is that of NiOEP, adopted in this work for Ni(HOEBC) (Table III).

they shift very far upon C_m H/D substitution, to 890 and 940 cm^{-1}, respectively. Immediately below these modes are ν_{20} (1218 cm^{-1}), ν_{14} (1182 cm^{-1}), and ν_{22} (1129 cm^{-1}), which shift *up* in the *meso*-d_4 isotopomer, to 1290, 1228, and 1169 cm^{-1}, respectively. The upshift results from relief of the interactions with ν_{21} and ν_{13}, when they cross over ν_{20}, ν_{14}, and ν_{22}. In NiOEP,[20] upshifts are also seen for ν_{14} and ν_{22}, but not for ν_{20}, which is at a much higher frequency, 1394 cm^{-1}, and therefore not subject to mode crossing.

Curiously, the ν_{10} and ν_{37b} modes are insensitive (1 cm^{-1}) to *meso*-deuteration in Ni(HOEBC) but shift 11 cm^{-1} in NiOEP, while the pyrrole half-ring modes ν_4 and ν_{41b} are nearly insensitive to *meso*-deuteration in NiOEP (4 cm^{-1}) but shift 17 and 30 cm^{-1} in Ni(HOEBC). Evidently, there is a reversal of the C_m–H bending contribution to these modes between NiOEP and Ni(HOEBC), but this reversal is not captured in the calculation, which predicts similar *meso*-deuteration shifts for these modes in NiOEP and Ni(HOEBC). A need for further alterations among interaction force constants is indicated.

Further refinement of the force field would be unproductive at this stage, however, in the absence of additional isotope data and in the absence of further structural characterization. This last point is emphasized in the RR spectral differences observed for Ni(HOEBC) in our polycrystalline (Figure 6) and solution phases (Figure 13). Not only are there dramatic intensity changes (ν_{14}, one of the strongest bands in the solid, nearly disappears in solution; ν_{10} shrinks, while ν_2 intensifies) but also ν_{10} shifts down by 9 cm^{-1} in solution, and the ν_2 and ν_{12} *meso*-d_4 isotope shifts diminish, from 11 and 42 cm^{-1} to 2 and 30 cm^{-1}. We infer that these alterations reflect a change in the porphyrin conformation which results in different excited-state displacements but also different normal mode compositions. The structure change may involve different out-of-plane distortions and/or different orientations of the peripheral substituents.

There are candidates for out-of-plane modes in the low-frequency RR spectra (Figures 11 and 12), i.e., 580 and 129 cm^{-1}, although the remaining bands have plausible in-plane assignments. There are also candidate bands for substituent C_1–C_2 or C_1–O stretching modes in the ~1100-cm^{-1} region (Figure 9), and a surprisingly strong band is seen for the 1268-cm^{-1} methylene twisting mode, assigned by analogy with NiOEP.[20] On the other hand, NiOEP and, likewise, NiOEC[12] and NiOEiBC[16] show quite strong ethyl C_1–C_2 bands at about 1025 cm^{-1}, the intensity being attributed to a hyperconjugative interaction with the porphyrin π orbitals,[20] but these bands are not observed for Ni(HOEBC). Some substituent modes also show up clearly in the IR spectrum, e.g., methylene twisting (1260 cm^{-1}), wagging (1315 cm^{-1}), and scissoring (1452 cm^{-1}), and methyl out-of-phase deformation (1384 cm^{-1}) and rocking (925 cm^{-1}) vibrations. We note that the IR assignments to the porphyrin skeletal modes are not as secure as the RR assignments because of spectral crowding and the lack of selective enhancement.

D. Comparison of the Vibrational Characteristics of the Nickel Complexes of Tetrapyrrole Chromophores. Since the reduction of pyrrole rings in metalloporphyrin affects the vibrational patterns of the parent porphyrin molecule through both the symmetry lowering and the reduced force constants of C_α–C_β and C_β–C_β internal coordinates, it is instructive to systematically compare the vibrational properties of the nickel(II) complexes of the di- and tetrahydroporphyrins, for which the observed frequencies are available.[12,16] These frequencies are categorized according to their respective local coordinates in Table V, which also illustrates the usefulness of the local coordinate concept in helping describe the collective vibrations of these complex but related molecules.

Inspection of Table V reveals that the frequencies of modes belonging to the same local coordinate but different symmetries are located in the same spectral region, excluding the expected changes caused by the C_β–C_β saturation. Thus, the $\nu(C_\alpha–C_m)_{asym}$ modes (ν_{10}, ν_{19}, and ν_{37}) for all four molecules occur consistently at the highest frequencies, while the number of high-frequency $\nu(C_\beta–C_\beta)$ modes directly reflects the degree of pyrrole saturation; the reduction of the C_β–C_β double bonds shifts one (NiOEC) or

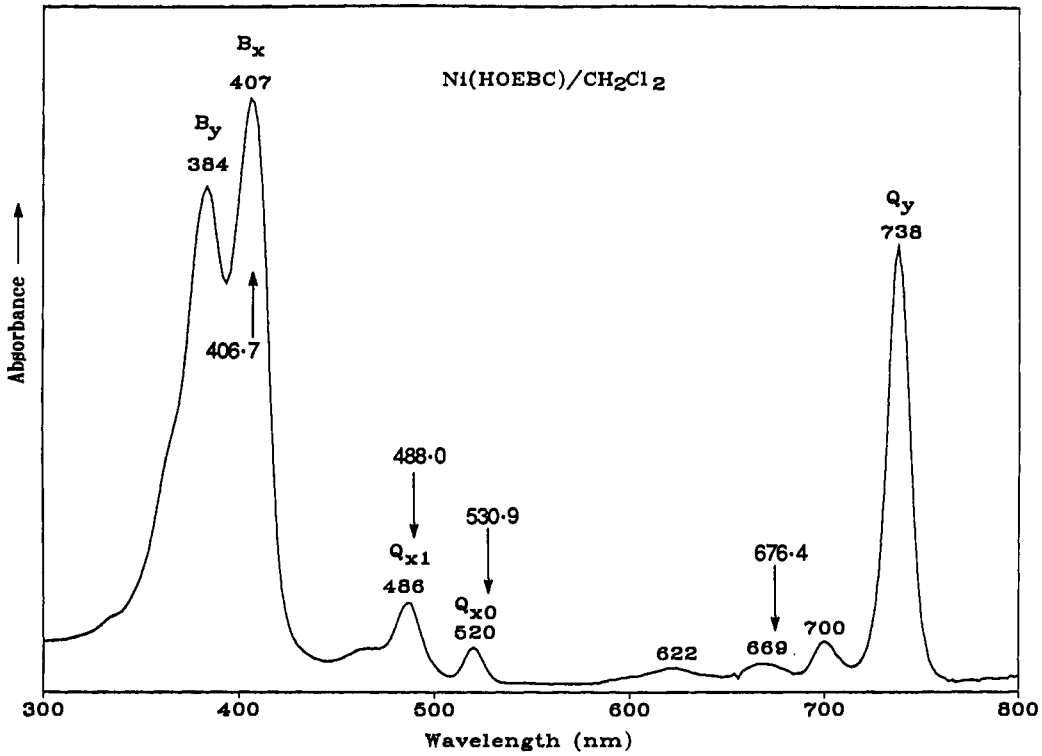

Figure 7. Electronic absorption spectrum of Ni(HOEBC) in methylene chloride. The arrows indicate the positions of excitation laser lines.

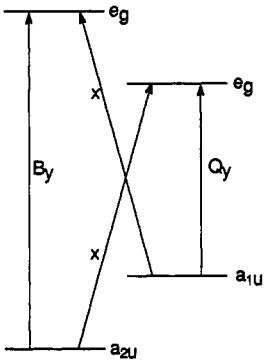

Figure 8. Frontier orbital diagram for metallobacteriochlorin.

two (NiOEiBC and Ni(HOEBC)) of the $\nu(C_\beta-C_\beta)$ modes to about 1110 cm^{-1}.

Modes between 1300 and 1500 cm^{-1} appear to be particularly sensitive to the symmetry lowering caused by the reduction of one or two pyrrole rings. In this region, there are two local coordinates, ν(Pyr quarter-ring) and $\nu(\text{Pyr half-ring})_{sym}$, which are combinations of C_α–N, C_α–C_β, and C_β–C_β stretching coordinates. We intuitively anticipate significantly altered frequencies for some of these modes, which are indeed observed in Ni(HOEBC). Although the pyrrole quarter-ring stretches ν_{20} and ν_{41a} are lowered from 1393 and 1346 cm^{-1} for NiOEP to 1218 and 1186 cm^{-1} for Ni(HOEBC), no frequency change is seen for NiOEC and NiOEiBC. This effect is attributable to the altered mode compositions in NiOEC and NiOEiBC, caused by the more extensive mixing in the lower symmetry framework (C_{2v} vs D_{2h}). The ν_{20} mode of Ni(HOEBC) is primarily localized on the pyrrolines, involving the out-of-phase stretchings of C^*_α–N* (15% PED) and C^*_α–C^*_β (41%), while the same mode in NiOEC is spread over the three pyrrole rings. Simiarly, the ν_{41a} (1198 cm^{-1}) of Ni(HOEBC) also consists mainly of the out-of-phase stretching of C^*_α–N* (16%) and C^*_α–C^*_β (43%).

E. Implication for Bacteriochlorophylls. Lutz[5a] previously proposed a set of empirical assignments for the RR spectral features of bacteriochlorophylls by comparison with the NiOEP modes. These assignments have recently been revised by Bocian and co-workers,[7h] who performed a normal mode analysis for copper methylbacteriopheophorbide, using the semiempirical quantum chemistry force field (QCFF/PI) method. These assignments were specified only in terms of internal coordinates, however. In view of the apparent usefulness of the local mode

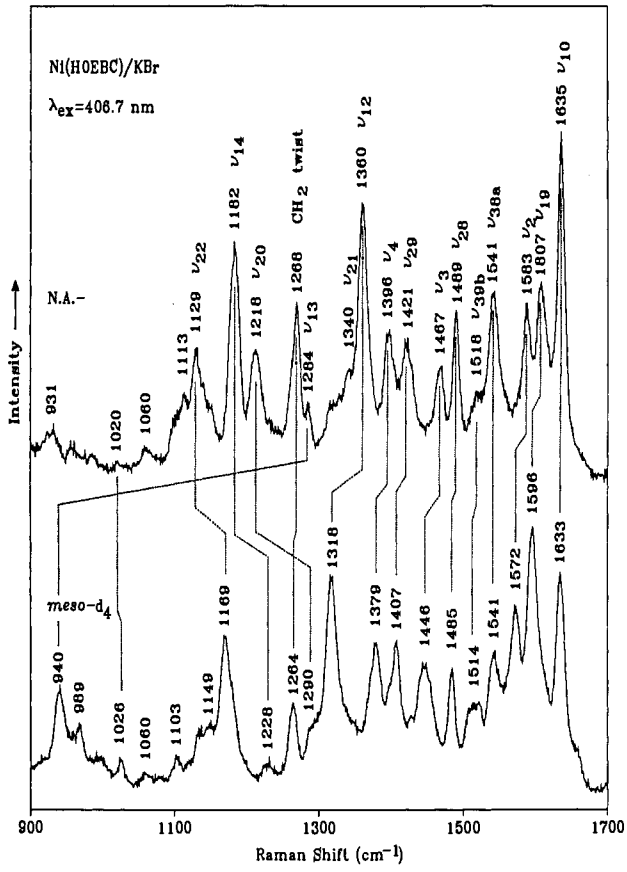

Figure 9. High-frequency resonance Raman spectra (407.7-nm excitation) of natural abundance (N.A.) Ni(HOEBC) and its *meso*-d_4 isotopomer in KBr pellet. The dotted lines correlate the same mode. Experimental conditions as in Figure 6.

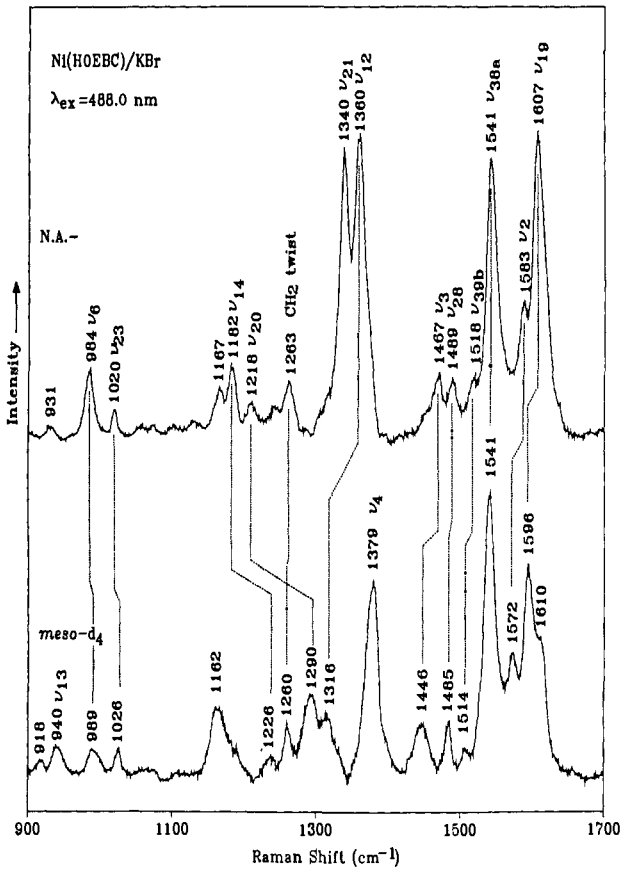

Figure 10. Same as Figure 9, but with 488.0-nm excitation.

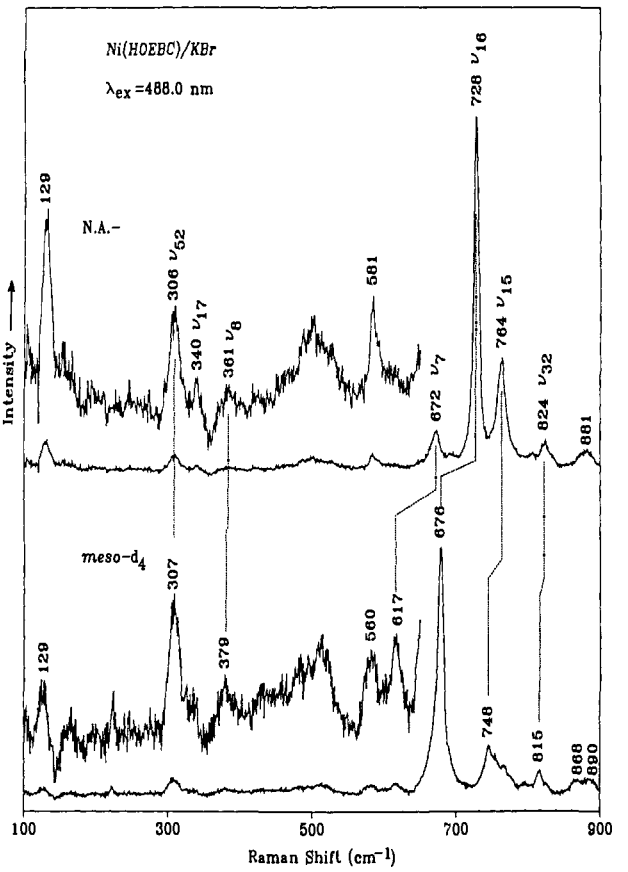

Figure 12. Same as Figure 11, but with 488.0-nm excitation.

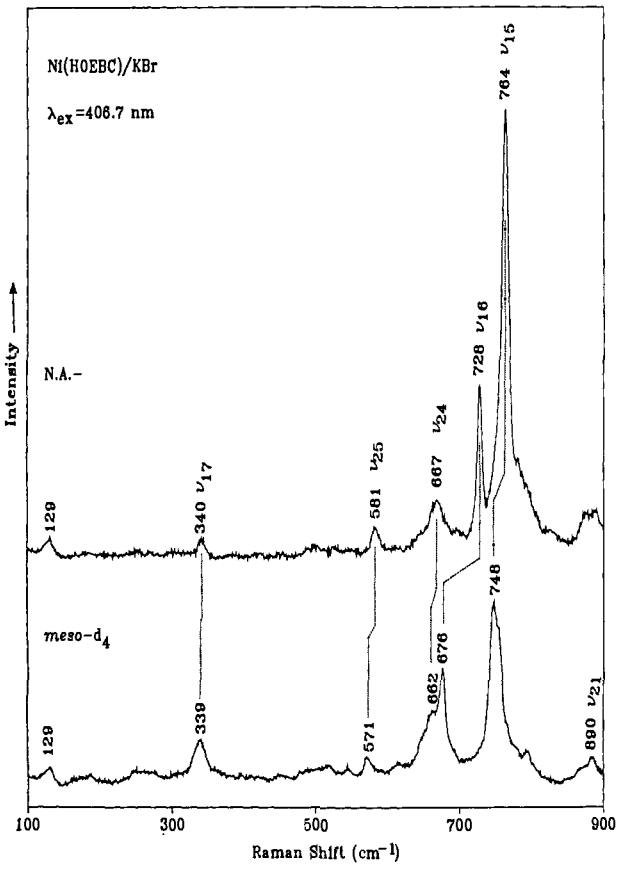

Figure 11. Low-frequency resonance Raman spectra (406.7-nm excitation) of natural abundance (N.A.) Ni(HOEBC) and its *meso-d*$_4$ isotopomer in KBr pellet.

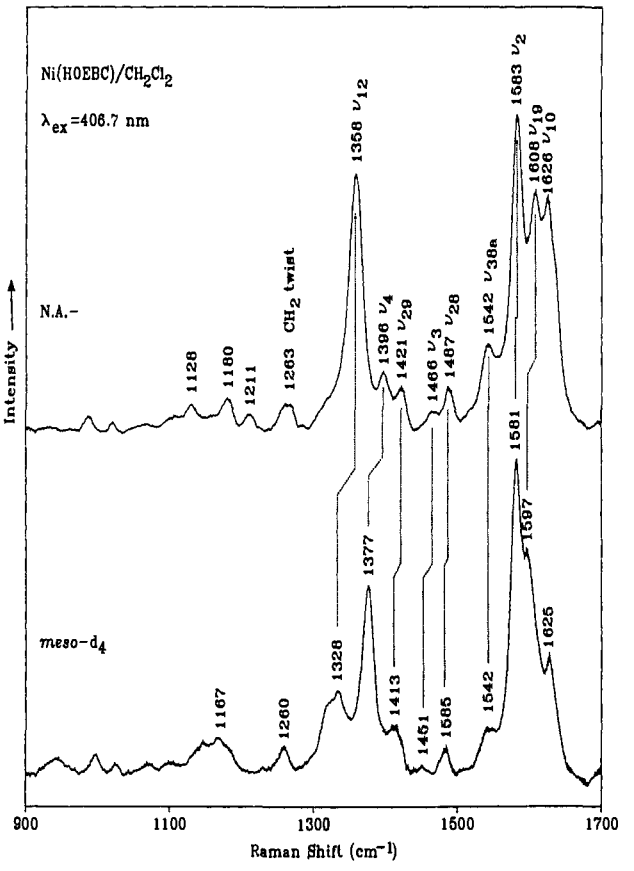

Figure 13. High-frequency RR spectra (406.7-nm excitation) of natural abundance (N.A.) Ni(HOEBC) and its *meso-d*$_4$ isotopomer in methylene chloride. The dotted lines correlate the same modes. Experimental conditions: 10 mW with cylindrical focusing, 2-s integration time, 120 scans.

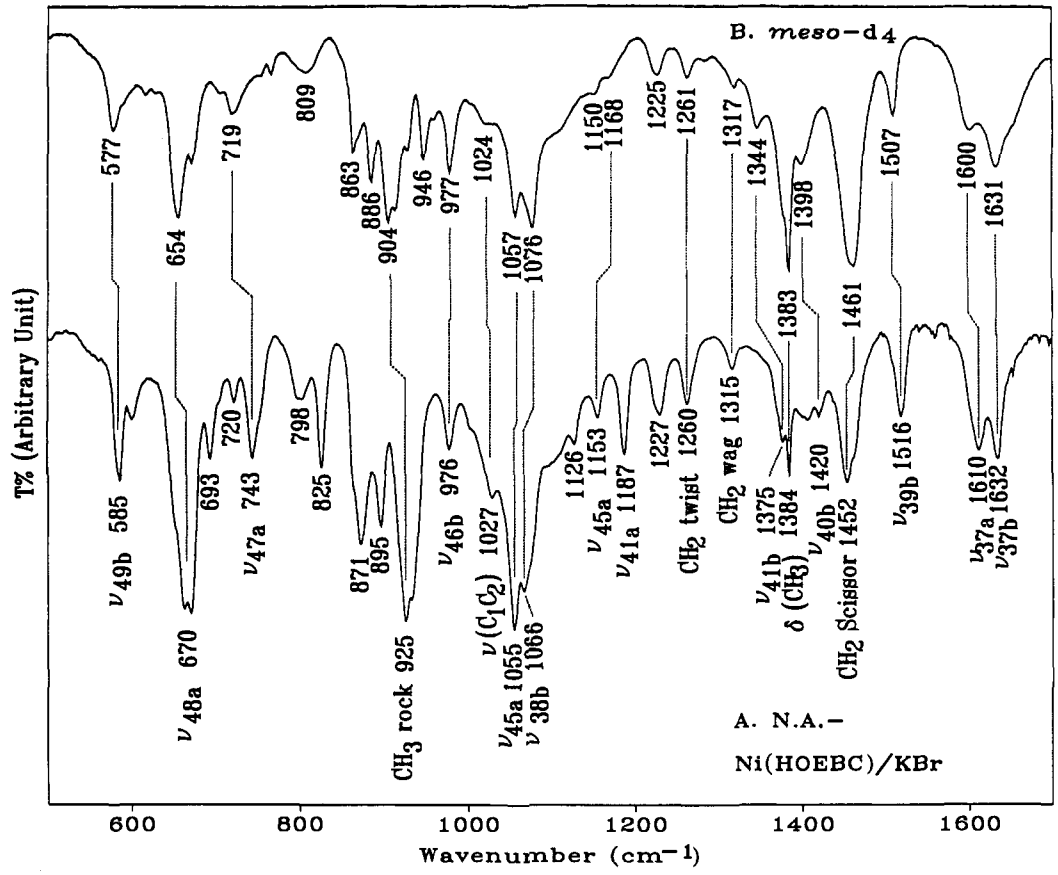

Figure 14. FTIR spectra of natural abundance (N.A.) Ni(HOEBC) and its *meso*-d_4 isotopomer in KBr pellet. Resolution: 4 cm^{-1}.

scheme for correlating the corresponding modes among porphyrins and hydroporphyrins, we propose the further correlation to bacteriochlorophyll modes given in Table VI. These assignments were made on the basis of selective enhancement patterns observed for RR bands excited in the region of the B_x and Q_x transitions and on the basis of the ^{15}N isotopic shifts. Also taken into account are the shifts for perdeuterated bacteriochlorophylls reported by Cotton and Van Duyne.[7f] It can be seen from the table that the ^{15}N shifts calculated for Ni(HOEBC) are quite close to those observed for bacteriochlorophyll a. This agreement provides strong support for the proposed assignments and suggests that the mode compositions for Ni(HOEBC) and bacteriochlorophylls are similar.

There are a few notable discrepancies between the present assignments and previous ones,[5a,7h] if the mode compositions are compared in terms of internal coordinates. The strong 1525 [1558 for Cu(bacteriopheophytin a)] cm^{-1} RR band was assigned to a mode composed mainly of C_β–C_β stretching but is reassigned to the pyrrole quarter-ring stretching. The observed 5-cm^{-1} ^{15}N shift is too large for a mode composed principally of the C_β–C_β coordinate. Another mode at 1215 cm^{-1}, previously assigned to the $\delta(C_mH)$, is more likely the pyrroline quarter-ring stretching mode (ν_{20}), judging from its ^{15}N shifts. Additional isotope data for bacteriochlorophylls are needed for more precise assignments.

Concluding Remarks

Almost all the in-plane skeletal modes of Ni(HOEBC), a model for bacteriochlorophylls, are assigned from the variable-excitation RR and FTIR spectra. The observed frequencies and *meso*-d_4 isotope shifts are reproduced with a force field developed for NiOEP, taking into account the structural differences between OEP and OEBC skeletons. The calculated eigenvectors provide insight into the vibrational characteristics of metallobacteriochlorins. A set of normal mode assignments for bacteriochlorophylls are proposed by analogy to those of Ni(HOEBC). The RR intensity enhancement pattern shows dominant Franck–Condon scattering in the B_x and Q_y regions and vibronic scattering in the Q_x region. The B_x excitation also reveals strong vibronic coupling between the B_x- and B_y-excited states.

Acknowledgment. This work was supported by DOE Grant DE-AC02-81ER-10861.